CHAPTER

12 Kinematic Models of Folding

In Chapter 11 we described the geometric characteristics displayed by folds in naturally deformed rocks. Geologists would like to understand the significance of these geometric features in terms of the mechanism of folding. To this end, they propose models to account for how folds might develop and then compare the characteristics of the model folds with natural folds. In this chapter, therefore, we discuss kinematic models of folding. We first consider various two-dimensional models for folding single layers (Sections 12.1 through 12.4), by which we can account for much of the geometric variation included in Ramsay's classification of folded layers. We then discuss two-dimensional models of multilayer folding (Sections 12.5 throngh 12.7), including kink and chevron folding, and fault-bend and fault-propagation folding. Finally, we discnss models for some three-dimensional aspects of folding, including the relationship between "drag folds" and the slip direction on associated faults, the geometry of superposed folds, and diapiric flow (Sections 12.8 through 12.10). Models such as these specify the motion of the deforming body but not, in general, the cause of the motion. For complete mechanical models of folding we must understand how stress and deformation are related, and we discuss these models in Chapter 20.

In order to discuss kinematic models of folding, we must introduce some basic concepts of deformation, and we restrict ourselves here to deformation that occurs in only two dimensions. After a **homogeneous deformation,** straight and parallel lines remain straight and parallel (Figure 12.1*A*, *B*; 12.2*A*, *B*), whereas after an **inhomogeneous deformation,** straight and parallel lines become curved and nonparallel (Figures 12.1*A*, *C*; 12.2*A*, *C*).

Simple shear is a two-dimensional constant-volume (in two dimensions, constant cross-sectional area) deformation that resembles the sliding of cards in a deck (Figure 12.1). If the deformation is homogeneous, the rectangular shape of the deck changes into a parallelogram (Figure 12.1*B*); if the deformation is inhomogeneous, the two sides of the deck normal to the cards become curved (Figure 12.1C). If a layer of rock is parallel to the shear planes, it is sheared, but it is not rotated by the deformation, and its length and thickness remain unchanged. Layers that are cross-cut by the shear planes are rotated, and they may be shortened and thickened, or lengthened and thinned, depending on their initial orientation.

Flattening is a deformation that can be represented by taking a square and shortening it parallel to one side while lengthening it parallel to the perpendicular side (Figure 12.2). If, in two dimensions, the deformation is homogeneous and the area stays constant, homogeneous flattening is called pure shear. After homogeneous flat-

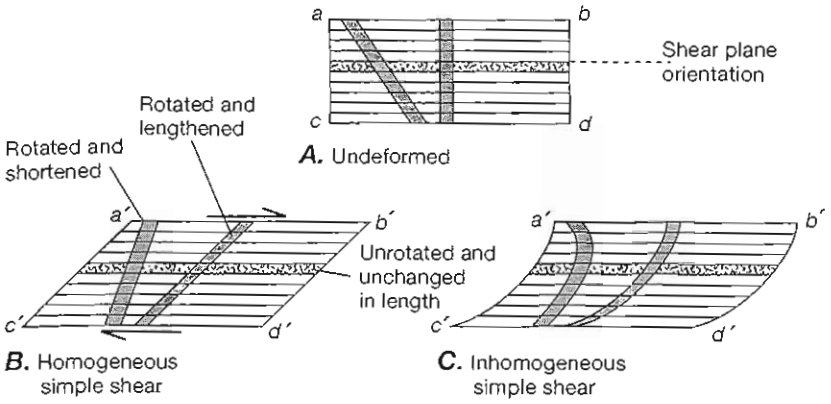

Figure 12.1 Geometry of simple shear. Rectangle *abcd* becomes deformed into *a′b′c′d′*. All displacements are parallel to the shear plane. Shaded bands represent different possible orientations of a layer relative to the shear planes.

tening, layers parallel to sides *ab* and *cd* are all unrotated and are shortened and thickened; layers parallel to *ac* and *bd* are also unrotated but are lengthened and thinned. Layers of any other orientation are rotated and may be shortened and thickened, or lengthened and thinned, depending on their initial orientation. In Chapter 15 we examine the geometry of deformation and strain in more detail.

The mechanical properties of the rocks involved in folding have a profound effect on the style of fold that develops. Qualitatively, we describe the relative rate at which a ductile material is able to flow at a particular differential stress in terms of its competence.[1] Under the same differential stress, a competent material deforms ductilely at a relatively low rate compared with an incompetent material. If similar-sized layers of competent and incompetent rock are forced to deform at a given rate, the differential stress is higher in the competent material than in the incompetent material. We discuss these mechanical properties more thoroughly in Chapters 18 through 20.

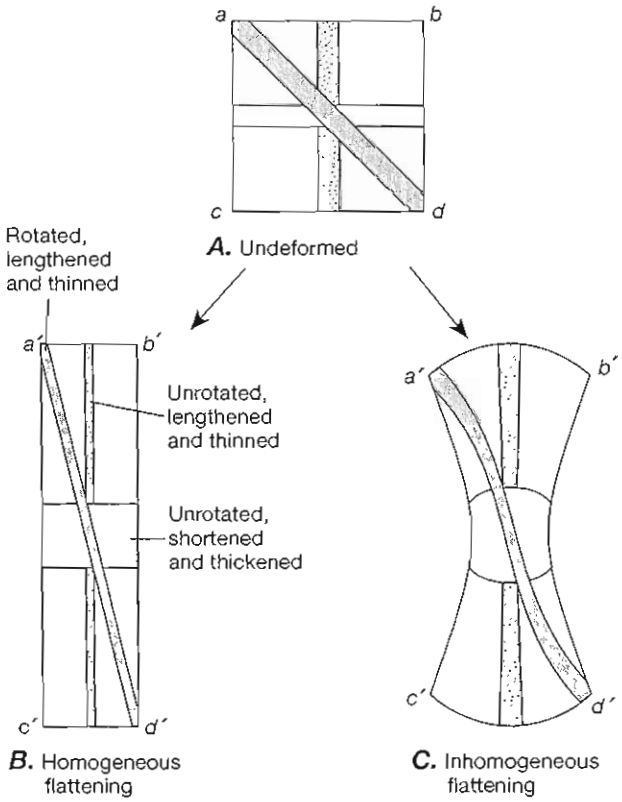

Figure 12.2 Geometry of flattening. The points *a*, *b*, *c*, and *d* become *a′*, *b′*, *c′*, and *d′* after deformation. Shaded bands parallel to *ac*, *ab*, and *ad* represent layers in different orientations with respect to the direction of flattening.

12.1 Flexural Folding of a Layer

Class 1B folds are a common feature of many fold belts (Section 11.5). The geometry of this class of folds may be explained by orthogonal flexure, flexural shear, and volume-loss flexure. Collectively, these models are called flexural folding. In all three models, the orthogonal thickness of the layer remains constant during folding, thereby producing class 1B folds. The class of the fold, therefore, cannot be used to distinguish the different mechanisms. The fold mechanisms differ, however, in whether the convex side of a fold is lengthened or remains constant and in whether its concave side is shortened or remains constant. Because the volume-loss mechanism can produce several geometries of fold, we consider it in a separate section (Section 12.3). Here we discuss orthogonal flexure and flexural shear.

Flexural folding of layers of rock can result from bending or buckling, which are two different ways of applying forces to the layers. Bending of a layer results from the application of pairs of forces that produce

[1] Some authors have used the term *ductility* in this sense. We eschew this usage because of the common engineering definition, also used by some experimental geologists, in which the ductility is the amount of ductile strain a material can accumulate before it fractures.

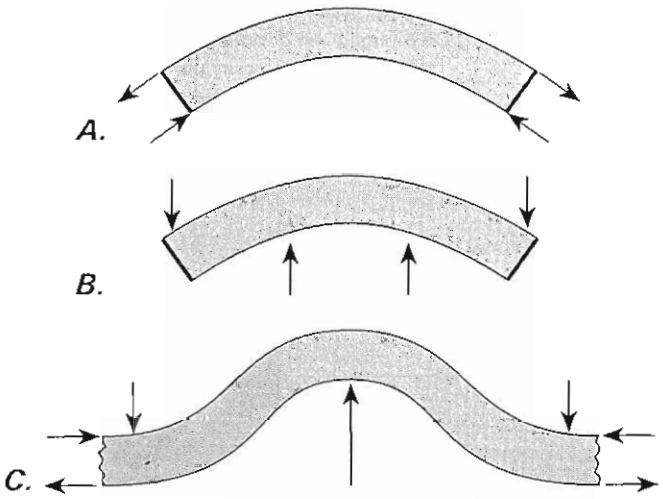

Figure 12.3 Flexure of a plate or layer by bending. Bending is caused by application of pairs of torques. A torque is a force that is applied normal to a lever arm and tends to make a body rotate. *A*. Bending moments created by pairs of equal and opposite forces applied parallel to the plate. *B*. Four-point loading: torques are created by forces applied perpendicular to the plate. *C*. One possible distribution of forces required to bend an infinite layer into a single localized fold.

equal and opposite torques that bend the layer into a fold. In pure bending, there is no net tension or compression, averaged over the layer, either parallel or perpendicular to it. Three possible systems of applied forces that provide such torques are shown in Figure 12.3.

Flexural folds can form by bending where a vertical force acts from below a layer to lift it into a fold. For example, the beds above a lenslike magmatic intrusion (called a laccolith) may fold in this manner. The fluid pressure of the magma provides a uniformly distributed upward pressure along part of the base of the layer. Monoclines or drape folds may also develop by bending (Figure 12.4) where faulting in the basement rocks provides the vertical force that bends the overlying strata into a monoclinal fold.

Buckling results from the application of compressive stresses parallel to the layer (Figure 12.5*A*, *B*). If the compressive stress is sufficiently large, the layer becomes unstable and buckles into a fold, either under compressive stresses alone (Figure 12.5*C*), or in association with additional torques (Figure 12.5*D*).

Buckling may be important in fold and thrust belts in which the compressive stress that drives the thrusting causes the layers to buckle, thereby shortening and thickening the thrust sheet. Folds in such belts, however, can also result from the sliding of thrust sheets up thrust ramps (Sections 6.2 through 6.4) and thus may form by a combination of bending and buckling (Section 12.7). Buckling also is of prime importance in the formation of ptygmatic folds.

A layer may respond to either bending or buckling loads by orthogonal flexure (Figure 12.6). In this kinematic process, all lines that were perpendicular to the layer before folding remain perpendicular to the layer after folding. In the profile plane, the surface of the layer on the convex side of a fold is stretched, and the surface on the concave side is shortened. The surface within the layer that does not change length during the folding is called the neutral surface. The orthogonal thickness of the layer remains constant all around the fold.

Orthogonal flexure should be characteristic of folds with low curvature developed in competent layers that are resistant to ductile deformation. As the curvature increases to high values, the orthogonality condition cannot be maintained.

A layer can also respond to bending or buckling by flexural shear, which is also called **flexural flow**. Folding is accommodated by simple shear parallel to the layer, and there is no stretching and shortening,

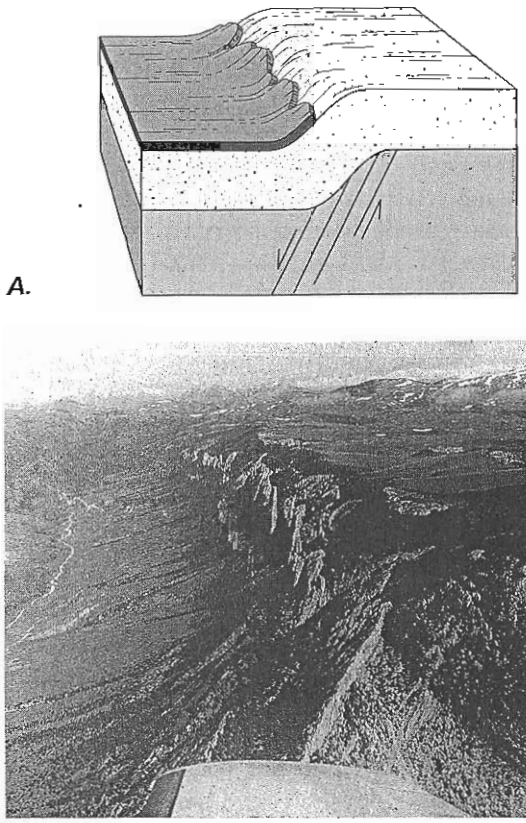

Figure 12.4 Monoclinal folds developed by bending. *A*. Diagram showing the formation of a monocline in sediments overlying a normal fault in basement rocks. *B*. Photograph of the Rattlesnake Mountain monocline, Wyoming.

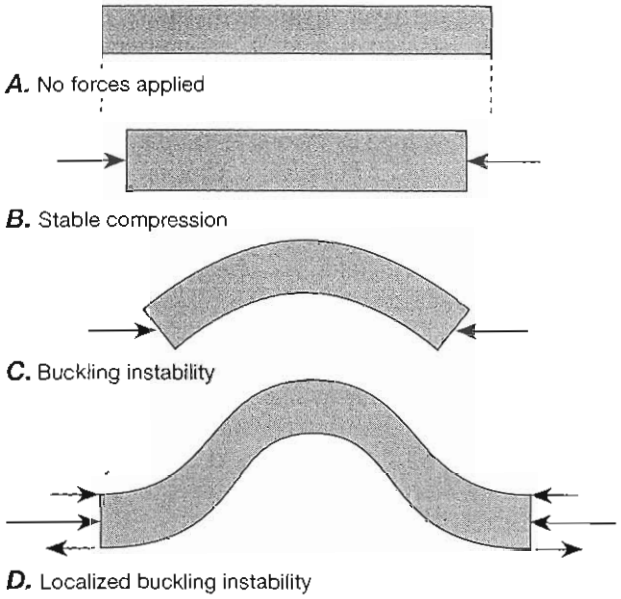

Figure 12.5 Flexure of a plate or layer by buckling. Equal and opposite forces are applied to opposite ends of the plate causing a compression of the plate.

respectively, of the convex and concave sides of the fold, as there is in orthogonal flexure.

Flexural-shear folding is analogous to the bending of a deck of cards (Figure 12.7) in that all the motion is parallel to the shear planes (represented by the cards) and the material on the convex side of a shear plane shears toward the fold hinge relative to that on the concave side. The sense of shear on the limbs of a fold therefore changes across the fold axial surface, and the magnitude of the shear decreases toward the hinge. The thickness of the body measured perpendicular to the shear planes is constant. Lines that were perpendicular

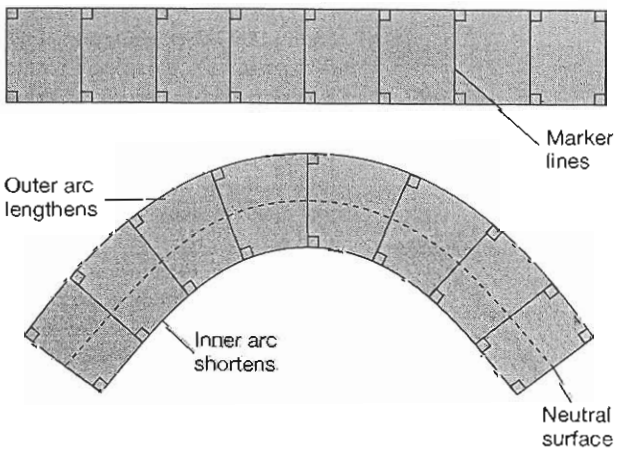

Figure 12.6 Geometry of orthogonal flexure.

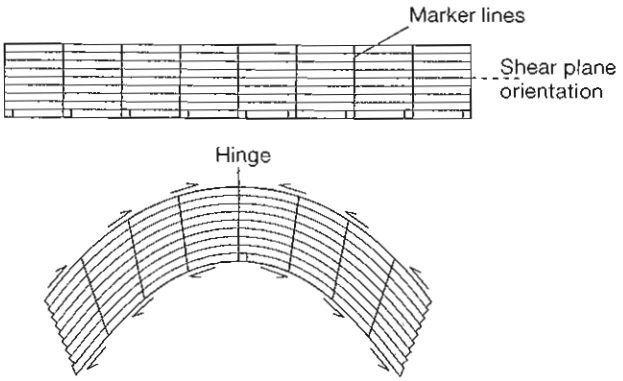

Figure 12.7 Geometry of flexural-shear folding.

to the surface of the layer before folding, however, do not remain perpendicular, except exactly at the hinge. During folding of a deck of cards, the length of individual cards is constant. Similarly, in flexural-shear folding, any length measured in the profile plane parallel to the shear planes is constant, so neither the convex nor the concave surface of the layer changes length.

Flexural-shear folding may occur instead of orthogonal flexure if the layer is less competent and therefore able to undergo ductile deformation more readily, or if the layer has a strong planar mechanical anisotropy,[2] such as fine interbedding of chert and shale or a strongly developed schistosity parallel to the layer.

12.2 Passive-Shear Folding of a Layer

In passive-shear folding, which is also called passive-flow folding or simply flow folding, the layer is highly incompetent and exerts no influence on the process of folding; it simply acts as a marker that records the deformation. Deformation takes place by inhomogeneous simple shear on shear planes that cross-cut the layer, and the amount and sense of shear vary systematically across the shear planes to produce the folded geometry. This process results in class 2, or similar, folds.

To illustrate the kinematics of the folding process, we can again refer to the model of the shearing of a deck of cards (Figure 12.1). In this case, however, the shear planes represented by the cards are not parallel to the layer being folded, as they are in flexural-shear folding, but instead cross-cut the layer (Figure 12.8). Along a given axial surface, the folded shape—and therefore the curvature—of the convex side of the folded

[2] The mechanical properties of a mechanically anisotropic material are different in different directions in the material.

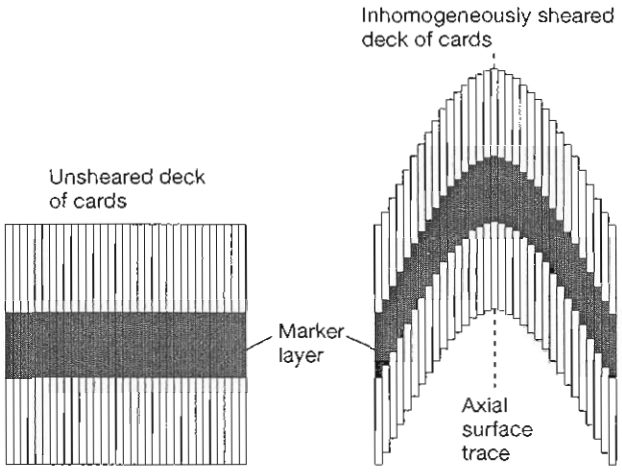

Figure 12.8 Passive-shear folding of a marker layer by inhomogeneous simple shear is approximated by "deck-of-cards" shear. The axial surface of the fold is parallel to the shear planes. The thickness of the layer parallel to the shear planes is consrant. The shape of rhe fold is exactly rhe same on the convex and the concave side of the layer.

layer is exactly the same as that of the concave side. Thus the hinge lines of folded snrfaces along the same axial surface must also lie on the same shear plane, and the shear planes are therefore parallel to the axial surface. Because there is no deformation within any given shear plane (none of the cards in the deck changes size or shape), the fold is cylindrical, and the axial trace thickness of the layer, which is measured parallel to the shear planes, is constant around the fold. These geometric characteristics are exactly those of class 2, or similar, folds.

In passive-shear folds, the fold hinge and the fold axis must parallel the intersection of the shear planes with the original layer orientation (Figure 12.9). The shear planes can be oriented at any nonzero angle to the layer, and the shear direction within the shear planes can be in any orientation except parallel to the layer being folded. As long as there is a component of shear across the layer, a fold can form. Thus the fold axis or hinge is not related to the direction of shear.

Natural fold geometries that come close to the geometry of class 2 folds are characteristic of deformation in high-grade metamorphic rocks, in salt domes, and in glaciers (Figure 11.1; see Sections 11.5 and 12.10) which suggests that this class of folds characterizes the deformation of incompetent materials. The model of passive-shear folding certainly requires incompetent behavior, but as we show in the next two sections, it is not the only mechanism that produces folds having a geometry very close to that of class 2.

12.3 Volume-Loss Folding of a Layer

Volume-loss folding is a mechanism by which folds can form or be amplified by the gradual removal of material from particular zones in a folded layer. The loss generally results from solution, so the folding process is also called solution folding. The volume-loss mechanism, howevet, does not result in a unique class of folds, beeause the fold geometry depends on the orientation of the zones of volume loss relative to the layer. Folds may form with class 1B, class 1C, or class 2 geometry. Volumė loss from diserete zones may result in the offset of beds, giving an appearance of shearing along the zones although in fact no shearing at all is required.

Three ideal fold geometries can result from volume-loss folding (Figure 12.10). Removing wedges of ma-

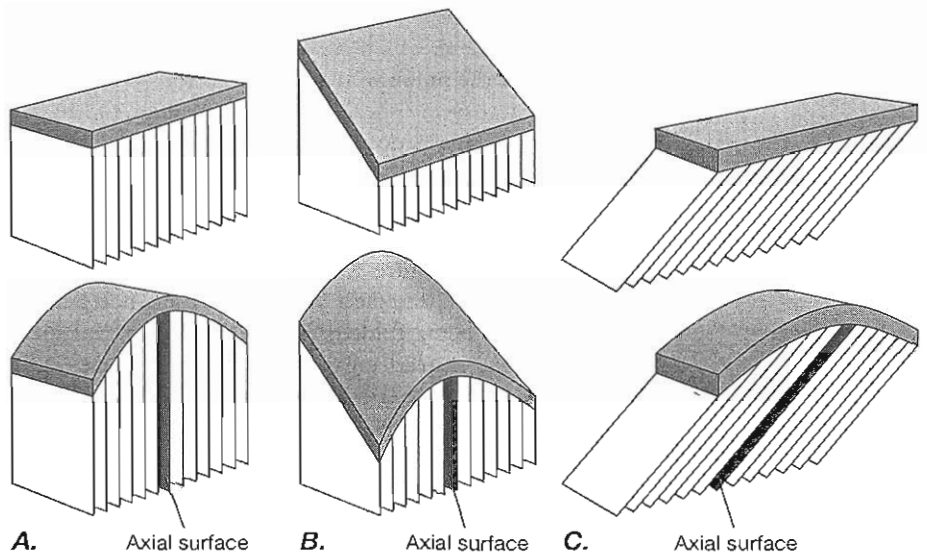

Figure 12.9 The orienrarion of the fold hinge for a passive shear fold is determined by the intersection of the shear planes with the original orienrarion of rhe layer to be folded. In parts A through C, the rop diagram shows rhe relationship berween the shear planes and the original orientarion of the layer. The bortom diagram shows the layer afrer folding. The shear directions could be any orientation in the shear plane except parallel to the surface being folded. The orienrarion of rhe fold hinge does not indicare the direction of shear.

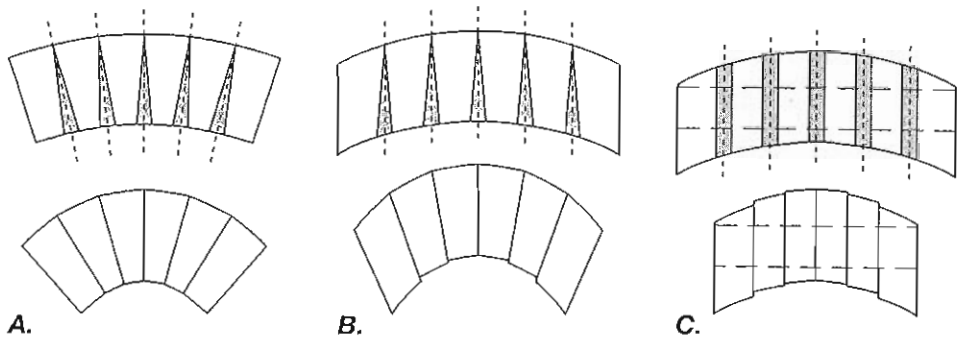

Figure 12.10 Volume-loss folding. The upper diagrams show the initial folds. The shaded areas are removed during intensification of the folds. *A.* Wedge-shaped areas of volume loss are symmetric about lines (dashed) that are normal to the surfaces of the layer. Both the convex and concave surfaces of the resulting fold are continuous and smooth. *B.* Wedge-shaped areas of volume loss are symmetric about lines (dashed) that are not normal to the surfaces of the layer. The convex surface of the resulting fold is smooth, but the concave surface has offsets that suggest shearing of the layer along the surface of volume loss. C. Lath-shaped areas of volume loss are parallel to one another and in general oblique to the layer. Both the convex and the concave surface of the fold show offsets that suggest shearing comparable to passive-shear folding.

terial symmetric about a line normal to the layer surface results in a class 1B fold in which both the concave and the convex surfaces are smooth (Figure 12.10*A*). Removing wedges of material symmetric about a line oblique to the layer produces a fold with the approximate geometry of a class 1C fold, but the concave surface of the fold is not smooth, and the discontinuous offsets along zones of volume loss could be misinterpreted as evidence of shearing (Figure 12.10*B*). For both models, the length of the convex side of the fold is unchanged by the loss of material, but the concave side of the fold is shortened.

Volume loss from parallel zones of constant thickness oriented oblique to an initial irregularity or gentle fold in the bedding can amplify a preexisting fold or irregularity, although it cannot produce a fold from a flat layer (Figure 12.10C). To this extent, it is geometrically comparable to deformation by homogeneous flattening, a process we discuss further in the next section. The result of this geometry of volume loss is a fold that approaches a class 2 style. The discontinuous offsets in both the convex and the concave surfaces suggest a fold formed by shearing on discrete shear surfaces, but no shearing is required.

Figure 12.11 provides an example of a fold that has been amplified by solution of material with a geometry comparable to that shown in Figure 12.10*B*. In the two photographs that make up Figure 12.11*A*, the bedding and the solution surfaces at a high angle to the bedding are visible, especially near the hinge zone of the fold. Figure 12.11*B* shows the fold restored to a more open configuration: The deformation caused by solution is undone, and the geometry of the concave side of the fold is returned to a smooth surface. The empty wedge-shaped gaps in the photo illustrate the volume of material removed along major solution surfaces.

12.4 Homogeneous Flattening of Folds in a Layer

With the models of folding considered so far, we have succeeded in producing class 1B, class 1C, and class 2 folds. Other kinematic models of deformation can also account for some of these classes, as well as for the other classes of folds in Ramsay's system. Flexural folding can accommodate only a limited amount of shortening before the folds are so tight that they cannot take up any further shortening. The model for passive-shear folding, moreover, does not permit any shortening whatsoever normal to the shear planes. We consider here the effects of homogeneous flattening (Figure 12.2*B*) superimposed on folds formed by the mechanisms discussed above.

It is impossible to create a fold in a perfectly flat layer by a homogeneous flattening, because in any homogeneous deformation, such a layer remains planar with parallel surfaces. Homogeneous flattening can, however, amplify an initial irregularity and change the geometry of a fold. An initial class 1B fold in a layer is contained within the square *abcd* (Figure 12.12). During homogeneous flattening normal to the axial surface, any part of the layer not exactly parallel to the direction of shortening is rotated away from that direction. In the

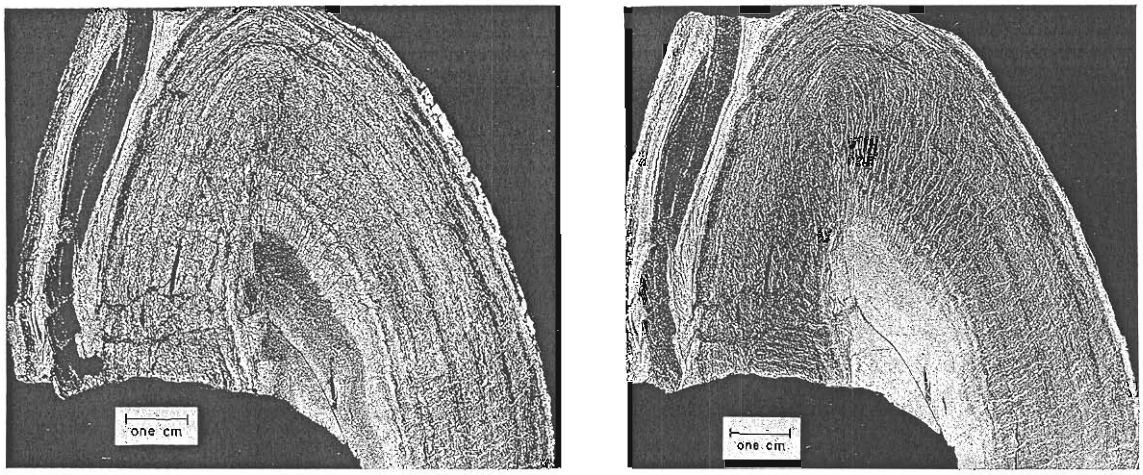

A.

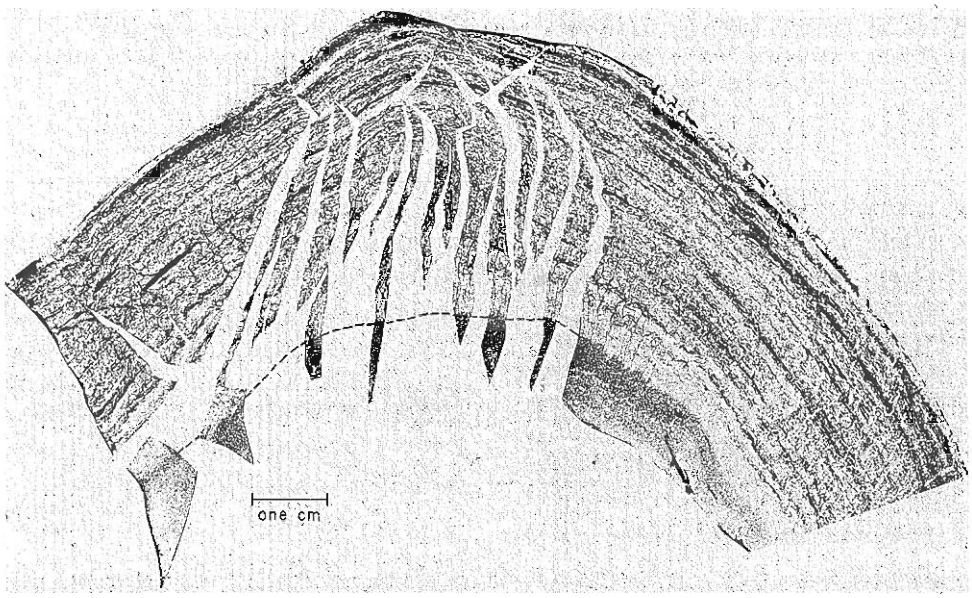

B.

Figure 12.11 Partial unfolding of a fold tightened by volume-loss (solution) folding. *A*. Negative photos of acetate peels emphasizing the cleavage (left) and the layering (right). *B*. The fold shown in part *A* restored to the condition of having a smooth surface on the concave side by opening the fold along major solution seams. The volume of material lost is indicated by the blank areas in the photo, along which the fold has been opened.

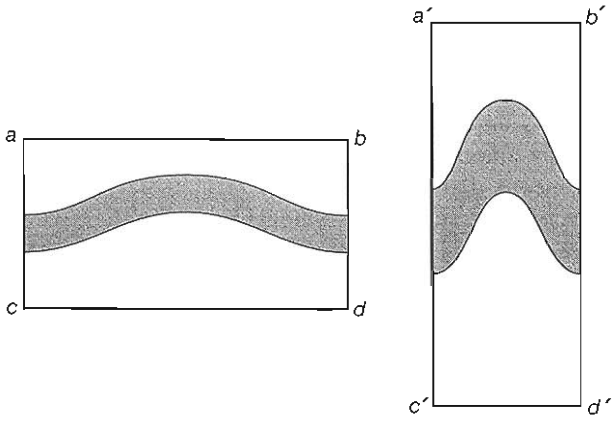

Figure 12.12 Intensification of folding by homogeneous flattening normal to the axial surface. The initial fold is a gentle class 1B fold. Progressive homogeneous flattening increases the amplitude and changes the fold into a class 1C fold.

fold hinges, where the layer is parallel to the shortening direction, the layer thickens in proportion to the change in length of the vertical sides *ac* and *bd* (Figute 12.12; see also Figure 12.2*B*). In the limbs of the fold, where the layer rotates toward a high angle from the shortening direction, its thickness decreases in a manner analogous to the decrease in length of the horizontal sides *ab* and *cd*. Thus after deformation, the layer is no longer of constant orthogonal thickness but is thicker in the hinge zone than in the limbs. The dip isogons still converge, so the cutvature on the concave side of the fold is still greater than on the convex side. The resulting fold has a class 1C geometry.

Consider now an initial fold of class 2 (Figure 12.13). If the axial surface trace is initially parallel to the vertical sides *ac* and *bd*, it remains parallel to these sides throughout the deformation. Although the axial trace thickness T changes during the defotmation, the change is the same everywhere and is proportional to the change in length of sides *ac* and *bd*. Thus the initial class 2 fold remains a class 2 fold under homogeneous flattening.

If a fold is subjected to a homogeneous flattening in a direction parallel to its axial surface and perpendicular to its hinge (Figure 12.14*A*), the layer thickness decreases in the hinge atea and increases on the limbs (Figure 12.14*B*). Dip isogons still converge, but the orthogonal thickness increases from hinge to limb. The resulting geometry is that of a class 1A fold.

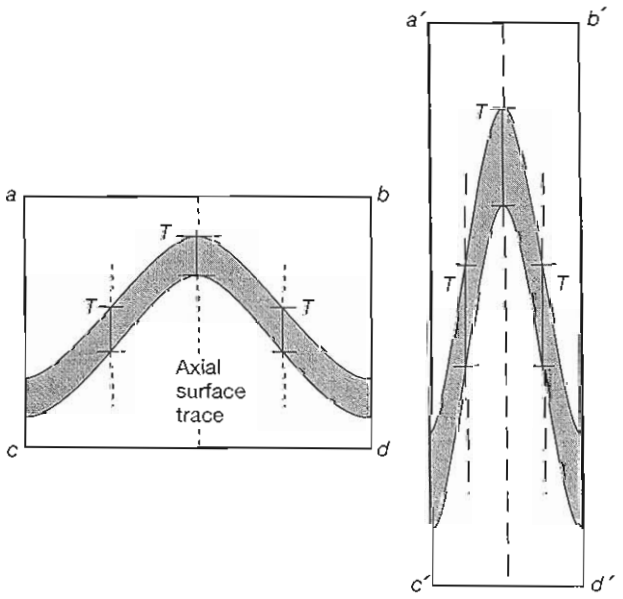

Figure 12.13 Intensificarion of a class 2 fold by homogeneous flattening normal to the axial surface. The initial square *abcd* is deformed into the rectangle *a′b′c′d′*. The axial trace thickness T is changed by the deformation to T' but remains equal all around the fold. The fold remains class 2.

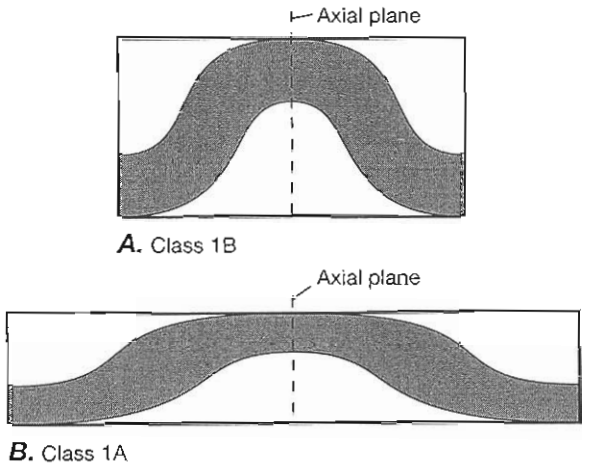

Figure 12.14 Homogeneous flattening of a class 1B fold parallel to the axial surface transforms the fold into a class 1A fold.

12.5 Flexural-Shear and Passive-Shear Folding of Multilayers

Most natural folding involves multilayered sequences of rocks that develop a more complex folding geometry than single layers. An important cause of this complexity is the difference in mechanical properties that can exist between adjacent rock layers. We take account of this factor in our models of fold formation by considering the mean competence for the whole multilayer and the contrast in competence among individual layers (Figure 12.15). First we consider a simple fold model that involves many layers of essentially the same high competence (high mean competence, low competence contrast). Then we eonsidet the effect of alternating thin incompetent and thick competent layers (high mean competence, high competence contrast). And finally, we

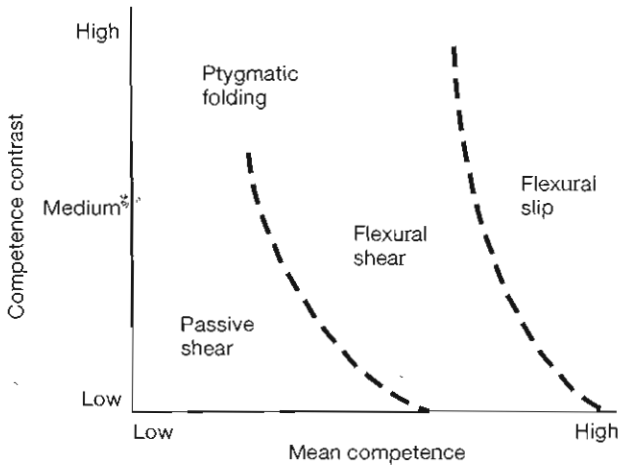

Figure 12.15 The dependence of the kinematic model of multilayer folding on rhe mean competence of the multilayer and on the contrast in competence between adjacent layers.

consider the effect of increasing the ratio of incompetent to competenr material in the multilayer (decreasing mean competence, high competence contrast).

If the competence contrast is zero, then the multilayer behaves as a single layer according to rhe models discussed in Sections 12.1 through 12.4. Even for sequences of layers of different competence, however, rhe package of layers may behave like a single unir with an effective thickness greater than any one of the individual layers. In that case, if a neurral surface develops wirhin the package, layers on the convex side of the neutral surface may be stretched and rhinned at the hinges, giving them a class 1A geometry.

A stack of layers can respond ro either bending or buckling by flexural-slip folding if the layers have essentially the same high competence (high mean competence) and if the friction between the layers is relatively low, allowing them to slide freely (this creares what is in effect a high competence conrrast between the layer surfaces and the layer interiors) (Figures 12.15 and 12.16). If each layer folds by orthogonal flexure, the concave side of each layer is shortened and the convex side is stretched. Thus, across a bedding surface, the layer on the convex side must slip toward the fold hinge relative to the layer on the concave side (Figure 12.16). This relative slip between layers is greatest on the limbs and decreases to zero at the hinge line, where it changes shear sense. The geometry of deformation is similar to flexural-shear folding (Figure 12.7), except that in flexural-shear folding, the shear is distributed uniformly across the folding layers, whereas in flexure-slip folding it is concentrated along the inrerfaces between layers. This type of folding produces a class 1B multilayer fold.

Sliding of the layers past one another commonly results in the development of liuear striations or mineral fibers (slickenside lineations or slickenlines) perpendicular to the fold axis on the bedding surfaces. The lineations are best developed on the limbs where the slip is a maximum, and they do not develop at all at the hinge (Figure 12.16*A*). The lineations (such as ℓ', ℓ'', and ℓ''' labeled on the fold in Figure 12.16*A*) plot on a stereonet along a great circle perpendicular to the fold axis f (Figure 12.16*B*).

If some degree of flexural shear occurs during folding (moderate mean competence, moderate competence contrast), theu some of the potential slip between layers can be taken up by shear within the layer, and the amount of interlayer slip decreases. If all the slip is distributed within the layers (moderate mean competence, zero competence contrast), the result is simply a multilayer flexural shear fold with class 1B geometry.

Many folds, however, consist of interlayered competent and incompetent lithologies of comparable thicknesses (moderate mean competence, high competence

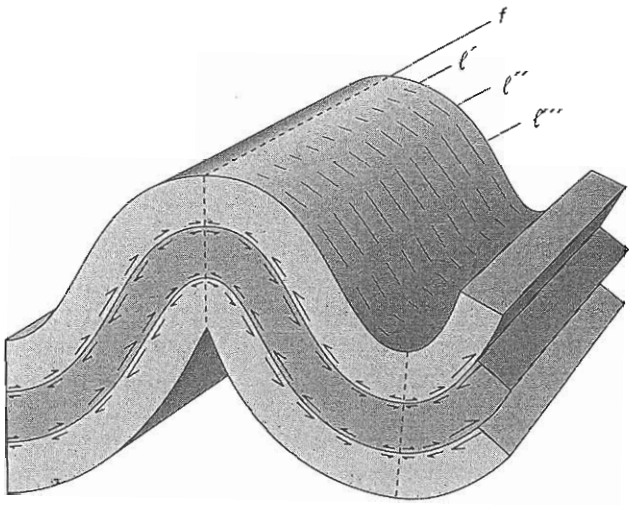

A.

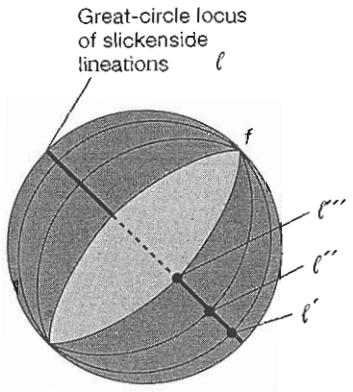

B.

Figure 12.16 Flexural-slip folding in a multilayer. *A*. Fold formed from an originally planar multilayer, showing relative displacement on layer surfaces. Layers on the convex side of a surface slip toward the hinge line relative to those on the concave side. The shear sense reverses across the hinge line. The lines on the surface of the layer indicate the orientation of slickenside lineations, and their lengths indicate relative amounts of slip. *B*. A stereonet diagram showing the range of orientations of the folded surfaces (shaded region) and the orientations of the lineations in those surfaces. The lineations lie on a great circle normal to the fold hinge f. The labeled lineations correspond to those shown in part *A*.

contrast). The competent layers as a group deform by flexural-slip folding, and the interlayer slip is taken up by deformation in the incompetent layers (Figure 12.17*A*). A multilayer class 1C fold develops, as indicated by the fact that on the average, the dip isogons converge toward the concave side of the fold, but not as strongly as for a class 1B fold. On the limbs of the fold, the incompetent layers are strongly sheared, whereas in the hinge zone they are simply flattened.

As the thickness of the incompetent layers increases relative to that of the competent layers (decreasing mean competence), the requirement that the adjacent competent layers nest tightly against one another becomes

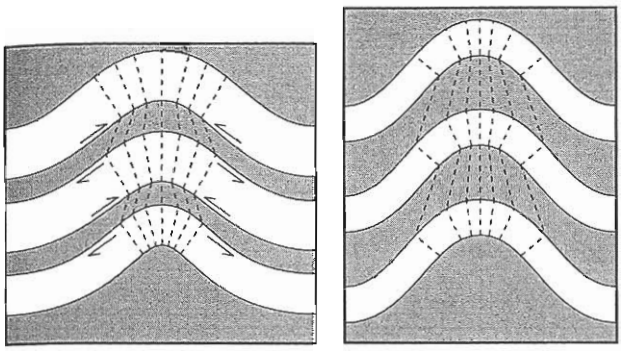

A. B.

Figure 12.17 Flexnral folding of interbedded competent and incompetent layers. *A*. A multilayer comprising three competent layers (unshaded) separated by thin incompetent layers (shaded). The dashed lines are dip isogons. Flexural folding of the competent layers is accommodated in the incompetent layer by shearing on the limbs and by flattening in the hinge of the fold. *B*. Flexural folding of a multilayer in which the incompetent layer is comparable in thickness to the competent layers. The multilayer class 2 fold comprises class 1B folds in the competent layers alternating with class 3 folds in the incompetent layers. Dashed lines are dip isogons.

less stringent. Competent layers still fold by the flexural folding mechanisms discussed for single layers, and they still dominate the development of the fold. The curvatures of the adjacent surfaces of two competent layers need not be the same, however, because the incompetent layer between the two competent layers flows in whatever manner is required to accommodate the difference in geometry; this generally involves layer-parallel shearing on the limbs and flattening in rhe hinge zone. Thus on the average, the dip isogons are not strongly convergent and could be parallel or even divergent. In an incompetent layer, the fold has a smaller radius of curvature on its convex side than on its concave side, the dip isogons diverge, and the axial trace thickness T_α decreases from hinge to limb (Figure 12.17*B*). These features characterize single-layer class 3 folds.

Thus a layered sequence can form multilayer class 1C, class 2, or class 3 folds by alternate development of class 1B folds in the competent layers and class 3 folds in the incompetent layers. The pattern of the dip isogons averaged over a number of layers may be convergent, parallel, divergent, or irregular, and this pattern defines the actual style of the multilayer fold.

If the incompetent layers are much thicker than the competent layers (low mean competence, high competence contrast), they dominate the large-scale deformation. The spacing berween the competent layers is so large that flexural folding of one competent layer does not affect the next one, and disharmonic ptygmatic folds develop (Figures 12.15 and 12.18). Although high-

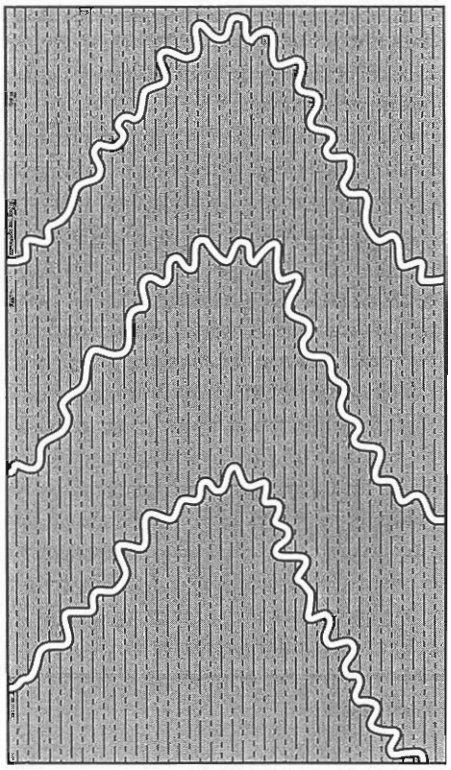

A.

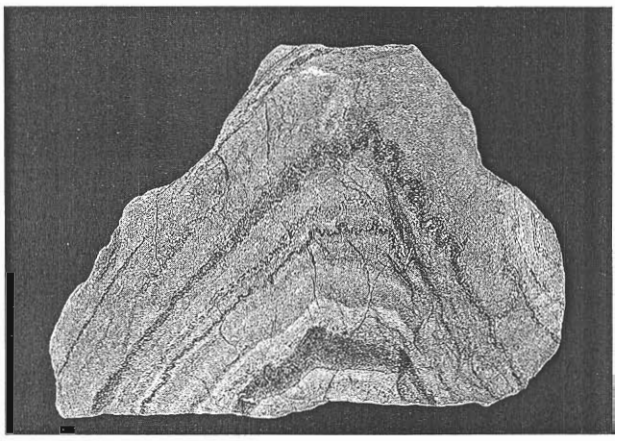

B.

Figure 12.18 Folding of a multilayer in which the incompetent layers are much thicker than the competent layers. Fold geometry is dominated by flow in the incompetent layers. *A*. A diagram of ptygmatic folds in thin competent layers in a fold whose geometry is dominated by flow of the incompetent material. *B*. Photograph of black amphibolitic layers ptygmatically folded in a metasedimentary rock from the Matterhorn Peak roof pendant, Sierra Nevada. The geometry is the same as in part *A*.

order folds in the individual competent layers are classes 1B and 1C, the geometry of the lower-order multilayer folds is close to class 2 and is dominated by ductile flow of the incompetent layers.

If the entire multilayer is made up of incompetent material with negligible difference in competence from layer to layer (low mean competence, low competence contrast), and if the layers do not slip past one another on their interfaces, then the multilayer is mechanically homogeneous and the layers simply act as passive markers of the deformation. Under these circumstances, the material should deform by passive shear with homogeneous flattening, rather than by bending or buckling, thereby forming folds that approximate class 2 style.

Thus flexural folding in multilayers requires competent layers and a planar mechanical anisotropy such as is provided by low-friction interfaces or thin incompetent interlayers (high mean competence, high competence contrast). Passive-shear folding in multilayers requires that an incompetent material dominate the mechanical behavior, and the effect of any competent layers is negligible (low mean competence, high to low competence contrast).

12.6 Formation of Kink and Chevron Folds

Folds with straight limbs and sharp hinges are chevron folds if they are symmetric and kink folds if they are asymmetric (see Section 11.5). They develop in strongly layered or laminated sequences that have a strong planar mechanical anisotropy, and they accommodate a component of shortening parallel to the layering or laminations.

Kink Folds

Kink folds occur in pairs with one short limb connecting two longer limbs (Figure 12.19). A kink band is the short limb between the two axial surfaces, which are the kink band boundaries. In the kink band, laminations are deformed and are rotated with respect to the undeformed material by an angle κ called the kink angle. We describe four different kinematic models of kink band formation, each of which involves a component of shearing parallel to the laminations as well as preservation of continuity of the laminations across the kink band boundaries. The models differ from one another in the way the kink grows and in the geometry of the deformation.

In two models (Figure 12.20), the kink develops by migration of the kink band boundary into the undeformed material. Folding by the migration of axial surfaces is different from any of the kinematic models of folding we have considered, although passage of the kink band boundary is accompanied by shearing of the material parallel to the laminations. Laminations in the undeformed and the kinked parts of the material maintain equal angles with the kink band boundary ($\gamma = \gamma_k$, Figures 12.19 and 12.20), and both the line lengths parallel to the laminations and the cross-sectional area remain constant. In Figure 12.20*A*, the kink nucleates along a line (*AB*) normal to the laminations and grows by rotation of the right boundary (*Ab*) counterclockwise about *A* and rotation of the left boundary (*aB*) counterclockwise around *B*, while *A* and *B* remain fixed points in the material. The kink angle κ increases continuously with kink growth. In Figure 12.20*B*, the kink nucleates along a line (*AB*) oblique to the laminations, and the two margins migrate in opposite directions while maintaining the same orientation. The kink angle κ is fixed by the angle between the laminations and *AB*, and it does not change with growth of the kink band. In both these cases, the deformation is of constant volume.

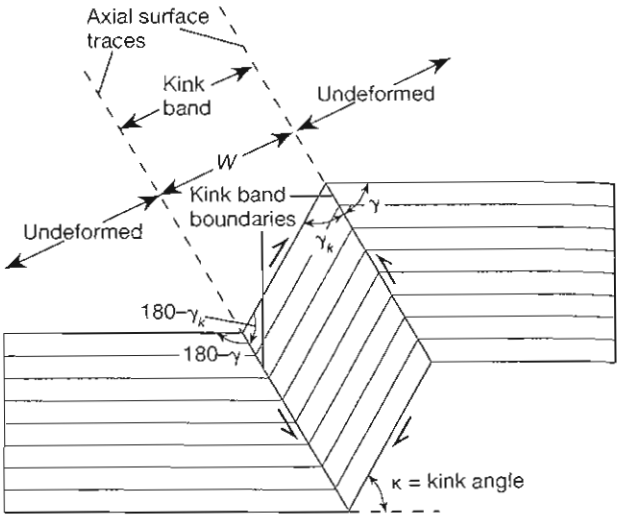

Figure 12.19 Geometry of a kink band, illustrating terminology. κ is the kink angle, w is the width of the kink band, γ and γ_k are the angles between the kink band boundary (the axial surface) and the undeformed and deformed material, respectively.

In the two other models (Figure 12.21), the kink band boundaries do not migrate but mark the fixed boundaries of a shear zone. As the kink develops, the kink angle κ increases, but the angles γ and γ_k are not equal: γ remains constant whereas γ_k decreases. In Figure 12.21*A*, kinking produces a deformation equivalent to homogeneous simple shear parallel to the kink band boundaries—and therefore is essentially like the passive-shear model. The width w of the kink band is constant, and the laminations are deformable. The lam-

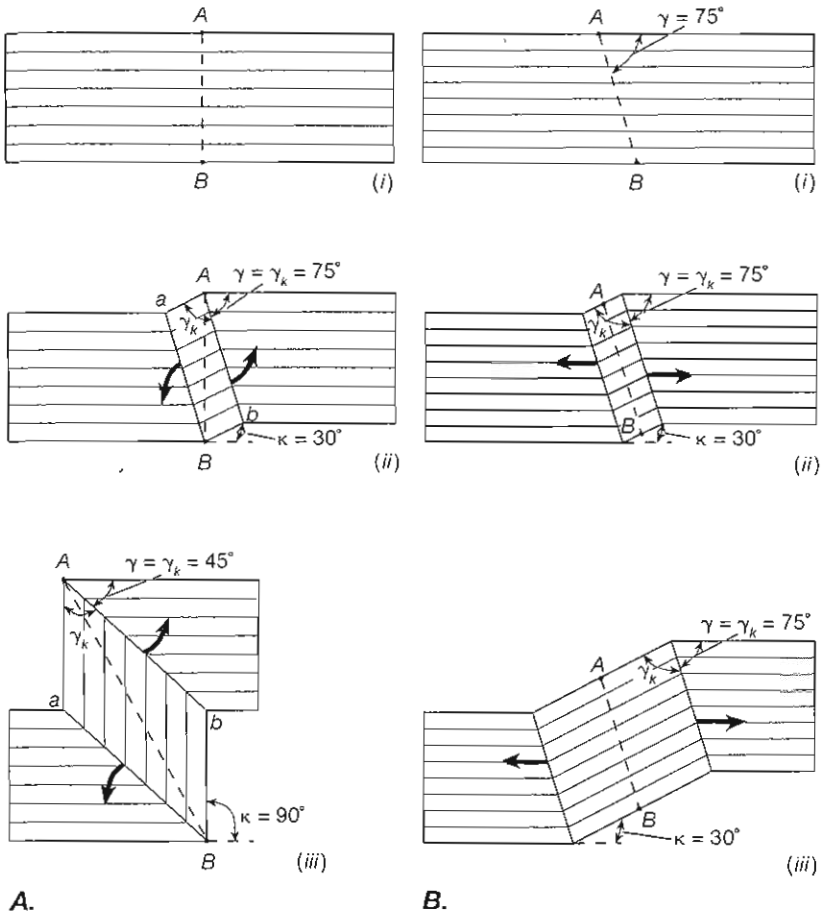

Figure 12.20 Kinematic models for the growth of a kink band by migration of the kink band boundary through the material. *A*. The kink band nucleates along the dashed line *AB* (i). It grows by rotation of the kink band boundary *Ab* counterclockwise about the fixed material point *A* and by rotation of the opposite boundary *Ba* counterclockwise about the fixed material point *B* (ii to iii). As the kink band grows, the kink angle κ increases. The angles γ and γ_k both decrease during kink band growth, but they remain equal. *B*. The kink band nucleates along the dashed line *AB* (i). The kink band grows by migration of the kink band boundaries in opposite directions into the undeformed material (ii to iii). As the kink band grows, the kink angle κ remains constant. The angles γ and γ_k remain equal and constant during kink band growth.

inations first rotate toward an orientation perpendicular to the kink band boundary, becoming shorter and thicker. With further rotation, the laminations lengthen and thin. The cross-sectional area remains constant throughout.

In Figure 12.21*B*, folding essentially involves a flexural-shear mechanism with shearing parallel to the laminations, which maintain constant length and width. As the kink develops, the laminations rotate toward an orientation perpendicular to the kink band boundary (Figure 12.21*B*, ii). The kink band becomes wider, and gaps open up between the lamination. With further rotation, the kink band becomes thinner again, and the gaps between laminations close. When γ_k decreases to the value of γ, no further kinking is possible (Figure 12.21*B*, iii). Because of the opening and closing of the gaps between the laminations, the cross-sectional area is not constant during the kinking.

Experiments on kink band formation indicate that kink bands do not develop along planes of high shear stress. Because the third and fourth models assume the kink band to be a zone of shear, the experiments suggest that these models may not be appropriate for describing natural deformation. Evidence points most strongly to the operation of the first and second models, either singly or together, in kink band formation. Some natural kink bands, however, show evidence of an increase in volume during deformation, such as accumulation of later minerals between separated layers. This indicates that in some cases, at least, model *B* in Figure 12.21 represents a component of the kinking mechanism. Model *A* in Figure 12.21 may account for some kink formation in high-grade metamorphic rocks.

Chevron Folds

Two kinematic models exist to account for the formation of chevron folds. In the first model, chevron folds develop where kink bands of conjugate orientation intersect (Figure 12.22). Transformation of the entire undeformed body into one completely filled with chevron folds requires a shortening of 50 percent. Although this mechanism has been observed to operate during the experimental deformation of phyllites, in naturally deformed rocks the observed shortening that results from kink folding rarely exceeds 25 percent, which is insufficient to form chevron folds by this mechanism.

Chevron folds can also develop by a process that is similar to flexural-shear folding (Section 12.1). In this

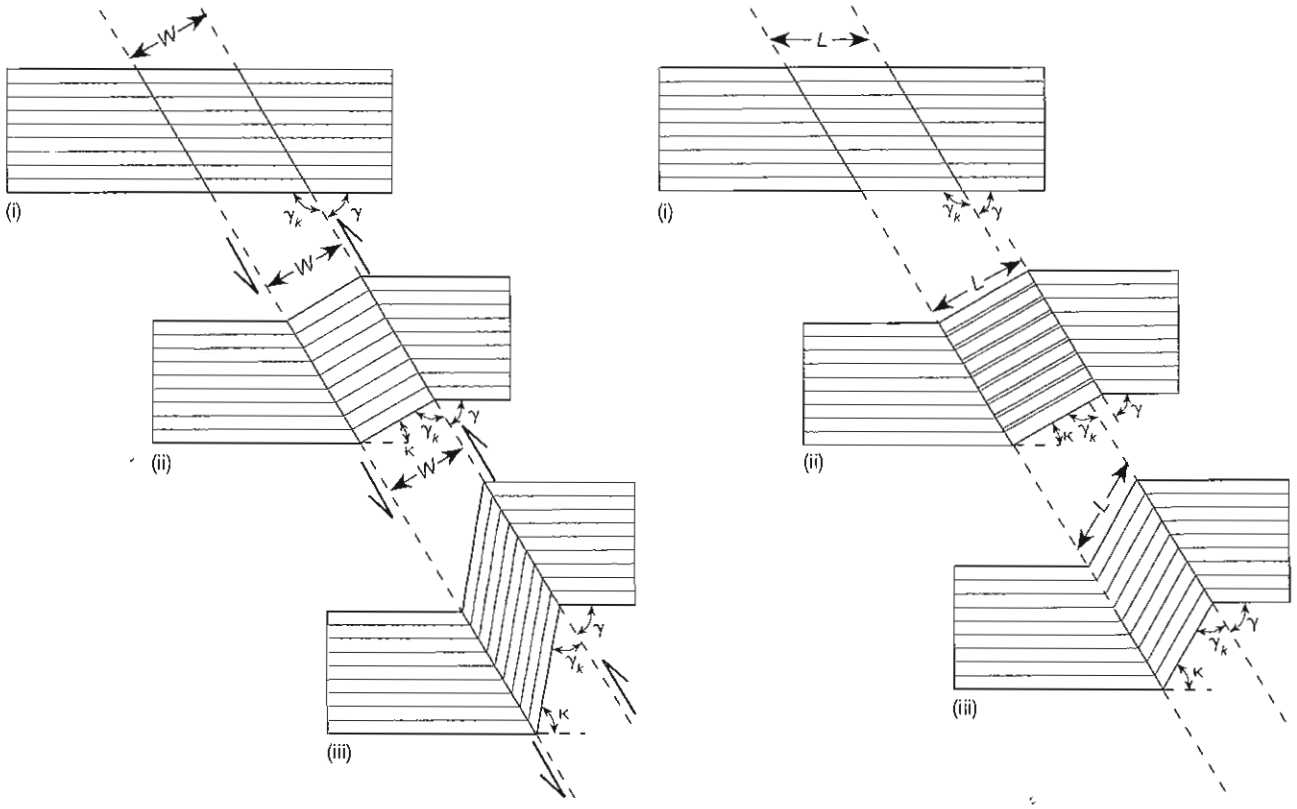

A. Kink band of constant width *W* **B.** Laminations of constant length *L*

Figure 12.21 Models for formation of a kink band in which the kink band boundary remains fixed in the material. *A*. Kink band growth by simple shear parallel to the kink band boundaries. The length of the laminations first decreases (i to ii), and their thickness increases until the laminations are perpendicular to the kiuk band boundary. With further rotation, their length increases and their thickness decreases (ii to iii). The width w of the kink band remains constant. As the kink band develops, the kink angle κ increases, γ remains constant, and γ_k decreases. Thus γ and γ_k do not remain equal. *B*. Formation of a kink band by rigid rotation of the laminations. The length of the laminations L in the kink band remains constant during kink band formation. Thus from (i) to (ii), where the width of the kink band increases as the laminations become perpendiculat to the kink band boundaty, and the volume increases as spaces open up between the laminatious. Ftom (ii) to (iii) the width decteases and the spaces between laminations close. Thus this is not a constant-volume deformation. As the kink angle κ increases, γ remains constaut, and γ_k decreases until $\gamma_k = \gamma$, at which point the spaces between laminations are completely closed and further kinkiug is impossible.

case, however, because the idealized laminations of the model are infinitesimally thin, the radius of curvature of the hinge does not have to change along the axial surface, as it does for flexural-sheat folding of beds of finite thickness. The result is a class 2 chevron fold formed by a flexural-shear mechanism.

Kink or Chevron Folding of Layered Sequences

Our idealized models have assumed that the kinked material is made of infinitesimally thin laminations and that shearing on the laminations tesults in a homogeneously distributed deformation. Such a condition is most closely approached in nature by foliated rocks such as slates, phyllites, and schists. Kink and chevron folds, however, also occur in thinly bedded rocks such as interbedded chert and slate. Whether a symmerric chevron fold or an asymmetric kink fold forms depends on whether the direction of shortening is parallel or oblique to the layering. The geometry of a chevron fold formed in a layered sequence that has low-friction bedding planes is illustrated in Figure 12.23. Formation of a class 2 fold by class 1B folding of the individual layers requires the opening of voids between the layers at the hinge. (When such voids are filled with secondary mineral de-

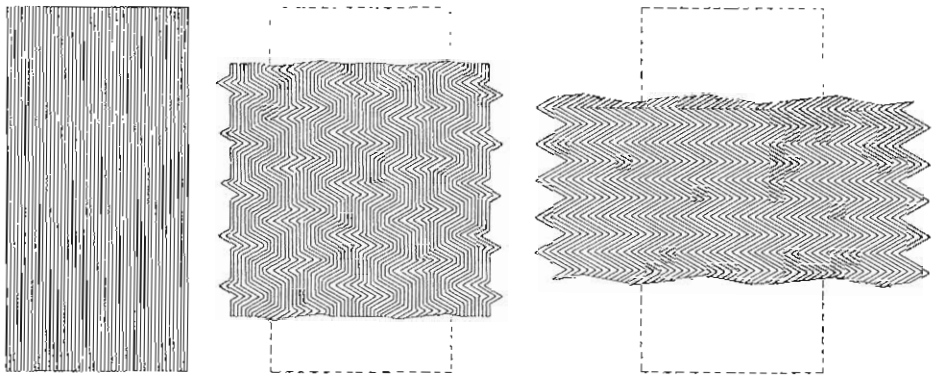

A. **B.** 30 percent shortening **C.** 50 percent shortening

Figure 12.22 Development of chevron folds by kinking. *A.* An undeformed block with a strong planar mechanical amisotropy. *B.* Shortening of the block parallel to the plane of weakness results in the formation of two sets of kink bands that have conjugate orientations. Chevron folds develop at the zones of interference between conjugate kink bands. *C.* As the widths of the conjugate kink bands increase, the area of interference, where the chevron folds develop, also increases until the entire block is filled with chevron folds.

posits, they are called *saddle reefs*.) If the competent layers are separated by incompetent material instead of low-friction surfaces, the incompetent material may flow from the limbs to the hinge zone to accommodate the mismatch in the fold form of the competent layers. This process once again produces multilayer class 2 fold geometry by alternate class 1B and class 3 folding in the competent and incompetent layers, respectively, as described in Section 12.5.

Our kinematic models do not explain why and under what conditions different folding mechanisms should operate. For example, they cannot resolve the question of why rounded folds form in some cases, and chevron folds form in others. In fact, we have not even explained why folds form at all, instead of the layers simply shortening and becoming thicker. To approach these questions, we must consider the mechanics of fold formation, which involves the mechanical properties of the material and the relationship between the stress and the deformation. We discuss the mechanics in Chapter 18 and Section 20.1 and address the application to folding in Sections 20.2 and 20.3.

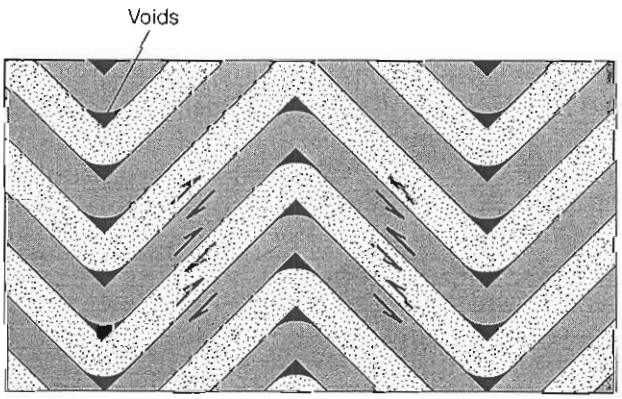

Figure 12.23 Chevron folding of layers of finite thickness by the flexural-slip mechanism introduces voids in the hinge zone (black areas).

12.7 Fault-Bend and Fault-Propagation Folding of a Multilayer

We describe in Chapters 5 and 6 on normal faults and thrust faults how bends in the fault surface (changes in dip or fault ramps) result in folding of the hanging wall block where it rides over the bend. Such fault-bend folds include the rollover anticlines on normal faults and the complex antielinal stacks above thrust duplexes. We can explain the fold geometry in many natural examples of fault-bend folding by using some fairly simple geometrical constraints and assumptions about the kinematics of layers being displaced over fault bends. Such constraints have proved extremely useful in interpreting the structure of several fold and thrust belts, and they are applicable to normal faulted terranes as well.

The kinematic analysis requires that we make the following assumptions:

1. No gaps are introduced as a result of slip along the fault plane.
2. Fault bends are sharp.
3. The orthogonal thicknesses of layers in the deformed block are preserved.
4. The lengths of layers in the deformed block are preserved.
5. Layers that have not been transported across a fault bend are undeformed.

These assumptions imply a bending model of folding that is accommodated by layer-parallel shear (that is, by the flexural-shear mechanism), that the folds have straight limbs and sharp hinges with a bluntness of zero, and that the folds are multilayer class 2 folds. Note that this is the one geometry for which flexural folding can produce a class 2 fold, and it is a basic property of models for kink and chevron folds (Section 12.6). In nature, the flexural shear actually may be approximated by flexural slip.

The geometry of the deformation in a fault-bend fold is illustrated for a fold concave toward the fault (an anticline) in Figure 12.24. For simplicity, the footwall block does not show the stratigraphy. The layers in the hanging wall block are shown folded across the fault bend. Dashed extensions of the layers indicate the layer geometry that would prevail if no deformation occurred in the hanging wall block. The angle through which the fault bends is β. The initial cutoff angle between the fault and the layers is θ, and ψ is the final cutoff angle. The interlimb angle ι is bisected by the axial plane, which is the geometry required to preserve constant bed thickness, and the folding angle is ϕ. From Figure 12.24, we can see that

$$\phi = 180 - \iota \qquad \phi = \psi + (\theta - \beta) \tag{12.1}$$

This geometry leads to the following equation, relating the fault-bend angle β to the interlimb angle ι of the associated fold if the initial cutoff angle is θ.

$$\tan \beta = \frac{-\sin (0.5\iota - \theta) [\sin (\iota - \theta) - \sin \theta]}{\cos (0.5\iota - \theta) [\sin (\iota - \theta) - \sin \theta] - \sin 0.5\iota} \tag{12.2}$$

For a simple ramp in a décollement for which $\beta = \theta$, this relationship reduces to

$$\tan \beta = \tan \theta = \frac{\sin \iota}{2 + \cos \iota} \tag{12.3}$$

These relationships determine the geometric evolution of a fault-bend fold. Figure 12.25 illustrates the two phases in the development of a fault-bend fold at a simple ramp. At the initial increment of displacement on the fault, two kink bands form, with kink band boundaries A and A' for one and B and B' for the other. Axial planes A' and B' are fixed in the hanging wall block at X' and Y', respectively, and they migrate with the block as displacement accumulates on the fault. Axial planes A and B are fixed in the footwall block at X and Y, respectively. Thus as displacement continues, material in the hanging wall block migrates through the axial surfaces A and B, and the kink folds grow. The first phase of development continues until the point Y' in the hanging wall block, to which axial plane B' is attached, reaches the point X at the top of the ramp. At this instant, the fold reaches its maximum amplitude, the axial surface B' becomes fixed at the point X in the

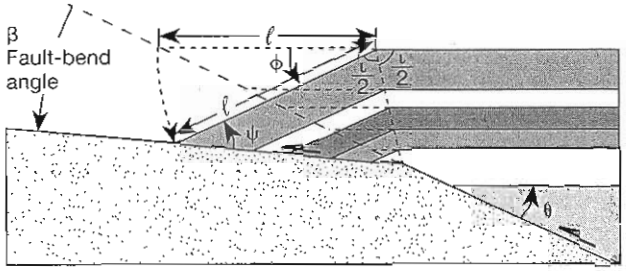

Figure 12.24 Geometry of deformation in a fault-bend fold. The angles are drawn in the positive sense for fault-bend folds that are concave toward the fault (anticlines). For fault-bend folds convex toward the fault (synclines), the angles ψ and θ, measured as shown, are considered to be negative. θ = the initial cutoff angle of the beds against the fault ($90° \geq \theta \geq -90°$); ψ = the final cutoff angle ($180° \geq \psi \geq -90°$); β = the angle of the bend in the fault plane ($90° \geq \beta \geq 0°$); ι = the interlimb angle ($180° \geq \iota \geq 0°$); ϕ = the folding angle ($180° \geq \phi \geq 0°$).

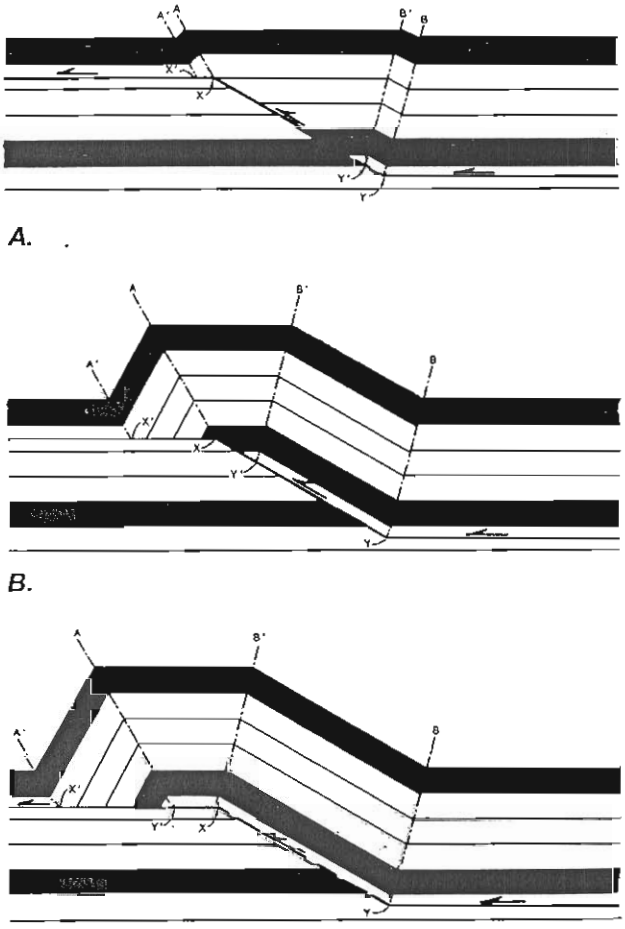

Figure 12.25 Development of a fault-bend fold at a simple fault ramp.

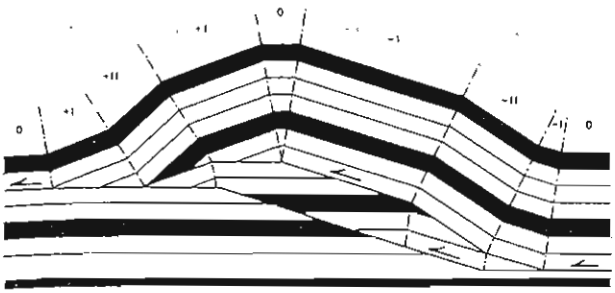

Figure 12.26 A faulr-bend fold resulting from imbrication of a thrusr faulr at a simple ramp and initiating a duplex srructure at depth. In this case, the number of increments of dip at the fronr and back of the fold indicates the number of imbrications on the faulr.

footwall block, and the axial surface A becomes fixed to the point Y' in the hanging wall block. The second phase of development begins with further displacement on the fault. Axial planes A' and A are now fixed in the hanging wall block and migrate with it, and axial planes B and B' are now fixed with respect to the footwall block at the bottom and top of the tamp, respecrively. Material in the hanging wall block migrates through these axial planes, becoming sheared as it passes rhrough B and unsheared as it passes through B'.

More complex models can also be treated, such as the development of fault-bend folds above imbricated thrust faults and dnplexes (Figure 12.26). Note that the dips of the layers change in a stepwise manner at the axial planes and that, in this case, the number of stepwise increases in dip at the front and back of the fold is an indication of the number of fault imbrications at depth. Thus under favorable circumstances the analysis of dip domains on fault bend folds at the surface can help constrain the geometry of complex fault structures at depth.

This same model applied to normal faults (Figure 5.5) predicts the existence of fault bend anticlines and synclines that reflect the geometry of fault surface at depth. A simple model of a listric normal fault with a roll-over anticline is provided by the left half of Figure 5.5B including only the main fault that cuts the surface and the connecting flat. The deformation associated with folding is accommodated by shearing on a set of synthetic faults parallel to both the main fault and the axial surfaces of the kink fold above the flat (cf. Figure 5.3).

Comparable folds also form in association with the propagation of a fault across a layered sequence, as illustrated in Figure 12.27. Where the fault turns upward to cut across the layering, a pair of kink folds form with kink band boundaries A and A' for one kink and B and B' for the other. The axial plane A' terminates at the tip line of the fault but is not parallel to the fault ramp. Thus it migrates through the material as the fault tip propagates. The kink band between A' and A accommodates the slip ahead of the fault. Axial plane B is fixed relative to the footwall block at the bend in the fault, and displacement on the fault causes material in the hanging wall block to migrate through B. Axial plane B' intersects axial plane A at the same stratigraphic level where the fault tip is located at any given time. Below this stratigraphic level, folding is complete because further displacement is taken up by slip on the fault, not by folding. Axial planes A and B' also migrate through the material as the fault tip propagates, but the axial plane formed from the merging of A and B' remains fixed in the hanging wall block and is displaced with it.

For the formation of a simple ramp in a thrust fault, under assumptions 1 through 4 above for fault-bend folds, a unique relationship can be obtained between the cutoff angle θ and the interlimb angle of the resulting fold ι.

$$2 \sec \theta - \cot \theta = -\cot \iota \qquad (12.4)$$

If folding becomes impossible at some point in this process (because, for example, of the resistance of a particular layer), the fault may propagate between the axial planes A' and A. If it cuts through above A', it leaves a right syncline in rhe footwall block, a feature commonly observed in narure and ascribed to "fault drag" rather than to fault-propagation folding.

Comparing Figures 12.25 and 12.27 reveals similarities in the folds formed by fault-bend folding and fault-propagation folding. The relationship between the interlimb angle ι and the initial cutoff angle θ, however, is different, as shown by Equations (12.3) and (12.4).

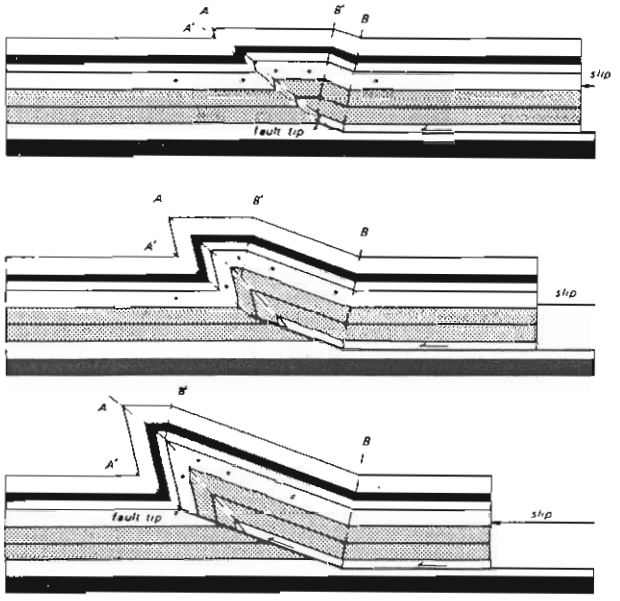

Figure 12.27 Development of a fault-propagation fold above rhe tip of a propagaring thrust fault.

For fault-bend folding, the maximum possible cutoff angle is $\theta = 30°$. For higher angles, the necessary deformation is impossible within the assumptions of the model. For fault-propagation folds, there is a unique relationship between interlimb angle and cutoff angle, and cutoff angles as high as 60° are permitted. In general, for a given cutoff angle, the interlimb angle for fault-propagation folds is smaller than is possible for common fault-bend folding, so the origin of a fault-related fold can in principle be determined. For most cutoff angles, which are less than 30°, tight folds result from fault propagation, and open folds from fault-bend folding.

These kinematic and geometric models for fault-related folding have proved very useful in the interpretation of the deep structure in a number of fold and thrust belts. Such interpretations must be based on surface mapping, well data, seismic data, and regional stratigraphic data, and they are not unique. The geometric requirements of the fold models, however, constrain how these data can be fitted into a viable model of the structure at depth.

If any of the assumptions for the model are violated in natural deformation, of course, the model does not provide reliable constraints on the reconstruction, and the distinction between the two fold origins may become blurred. Beds may deform by nonlayer-parallel shear, they may thicken or thin by homogeneous deformation, or the volume of part of the section may be changed by solution of material. Some aspects of nonlayer-parallel shear can be included in the model, but most other types of deformation do not yield unique geometric constraints. In such cases, inconsistencies in the reconstructions can point to situations in which the assumptions of the model do not apply.

12.8 "Drag Folds" and Hansen's Method for Determining the Slip Line

When rocks are subjected to shear, layers in the rock commonly form asymmetric folds whose sense of asymmetry reflects the sense of shear of the deformation. Such folds are commonly called drag folds, the implication being that the velocity gradient in the shear zone has dragged the layer into a fold. Characteristically they are noncylindrical, asymmetric, and disharmonic. Because hinge orientations depend on the original orientation of the layer relative to the shear plane and on local inhomogeneities in the flow, they can vary widely and need not be linear (see, for example, the folds in the salt bed in Figure 12.34*A*). Thus the hinge orientations do not indicate the slip direction. The hinges may form parallel to the shear plane; if they do not, subsequent simple shearing tends to rotate them toward parallelism with both the shear plane and the slip direction. More complex geometries of flow than simple shearing, however, can rotate fold hinges forward being either parallel or perpendicular to the direction of flow.

The sense of asymmetry of any "drag fold," whether its hinge is curved or straight, must be consistent with the sense of shear in the zone. This relationship of fold asymmetry to shear sense is the basis of the Hansen method of determining the slip direction.[3] If all hinge orientations are plotted on a stereonet with their appropriate shear senses, then they should lie approximately along the shear plane (Figure 12.28*A*, *B*). The separation angle, across which the shear sense changes, contains the slip direction, and the asymmetry of the folds defines the sense of shear of the deformation (Figure 12.28*B*). The hinges closest to being parallel to the slip direction (hinges 1 and 3, Figure 12.28) constrain the possible slip orientation, because fold hinges on opposite sides of the slip line must have opposite shear senses.

[3] A complete discussion of the application and pitfalls of this method can be found in Hansen (1971).

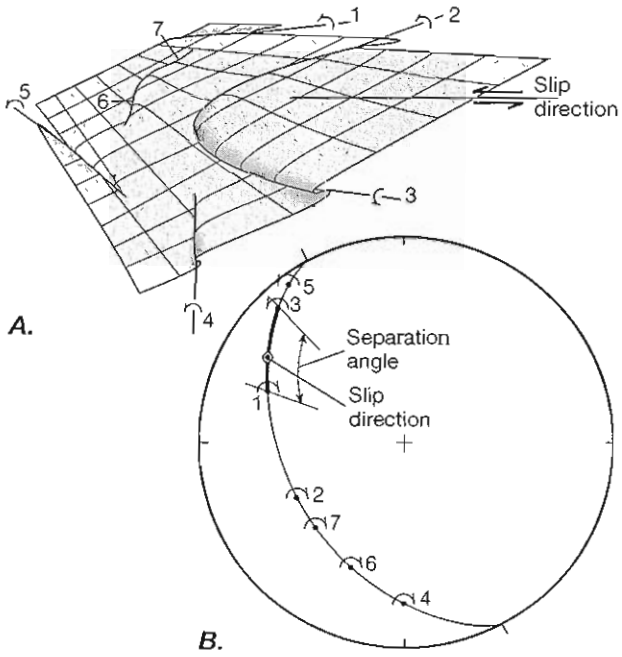

Figure 12.28 Hansen's method for slip line determination in folded layers subparallel to the shear plane. *A*. Fold hinges numbered 1 through 7 have a variety of orientations. The asymmetry of any part of a fold hinge, however, is consistent with the sense of shear. Because fold hinges 2 and 3 lie on opposite sides of the slip direction, they have opposite shear senses. *B*. On a stereonet, the hinge orientations plot parallel or subparallel to the shear plane, and the asymmetry of the folds changes sense across the separation angle, which must contain the slip direction. The sense of fold asymmetry defines the shear sense of the deformation.

12.9 The Geometry of Superposed Folding

In complexly deformed areas such as the central core regions of orogenic belrs, folded layers of rock commonly display a geometry indicating thar earlier folds have been folded by one or more sets of later folds. Such multiple foldings are referred to as superposed folding, and the different sets of folds are called generations of folds. A first generation of folds is refolded by a second generation and by all subsequent generations.

In discussing superposed folds, we need a noration to describe the successive surfaces and hinges formed. The terminology is illusttated in Figure 12.29. Surfaces are labeled S. Bedding is S_0, and the axial surfaces of first, second, and higher generations of folds, which are assumed to form as planar surfaces, are designated S_1, S_2, and so on. Fold hinges are labeled f. The fold hinges of successive generations are f_1, f_2, and so on. It is also useful to include with the fold hinge symbol a designation of the surface being folded. Thus the fold hinge $f_1^{S_0}$ means a first-generation fold hinge in the S_0 surface (bedding). Second-generation folds develop in the already folded bedding S_0 and in the first-generation axial surfaces S_1. Thus second-generation fold hinges in these surfaces are labeled $f_2^{S_0}$ and $f_2^{S_1}$, respectively (Figure 12.29).

The basic patterns of orientations of fold hinges and axial surfaces that result from the superposition of two generations of folding can be analyzed according to fairly simple geometric rules. In general, the youngest generation of folding has planar axial surfaces. The axial surfaces of older generations are folded by all

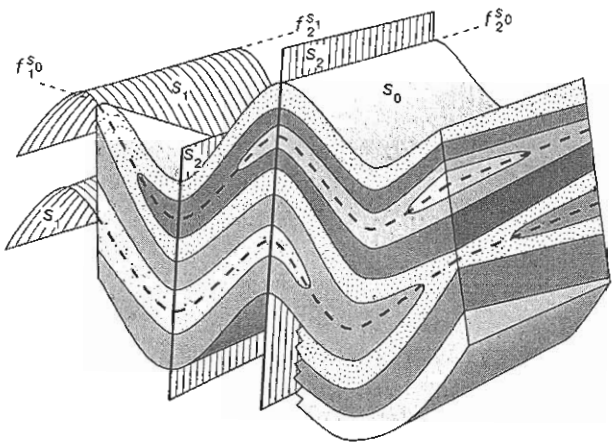

Figure 12.29 Geometric elements of a refolded fold. The first-generation folds are folds in S_0 with fold axis $f_1^{S_0}$ and axial surface S_1. The first-generation folds are refolded by second-generation folds that have axial surface S_2. Second-generation fold axes develop in S_0 ($f_2^{S_0}$) and in S_1 ($f_2^{S_1}$).

younger generations. After two generations of folding, for example, second-generation folds are developed in both the bedding S_0 and the eatlier generation axial surface S_1, and both have the same planar second-generation axial surfaces S_2 (Figure 12.29). Earlier generation fold axes commonly behave like passive linear features and are rotated by later generations of folding. The rotated axes develop predictable patterns that depend on the initial fold axis orientation and the geometry of the later deformation. We discuss some of these patterns in Section 16.1 (Figures 16.1–16.3). Although the youngest generation axial surfaces are commonly planar, the associated fold axes develop in a range of orientations depending on the initial orientation of the surface being folded (compare fold axes in Figure 12.9 *A, B*). They are related to one another only in that all the youngest generation fold axes must lie within the youngest generation axial surface. Although real folds can be considerably more complicated than these idealized relationships suggest, analyses of the geometrical relations have allowed complex sequences of superposed structures to be unraveled. The details of the procedures are beyond the scope of this book.

If second-generation folding is flexural folding of approximately the same scale as first-generation folds, which would be expected for competent layers, the geometry resulting from the superposition does not conform neatly to the principles we describe above. Figure 12.30*A, B* shows the results of the experimental superposirion of two generations of flexural folds in a stiff, puttylike material, and they illustrate the complexity of the superposed geometry.[4] Although in Figure 12.34*B* many of the second-generation fold hinges ($f_2^{S_0}$) lie close to the second-generation axial surface (S_2) (Figure 12.30*C*), rhe first-generation folds are widely scattered and show no simple geometric pattern.

If the second generation of folding occurs by passive shear and is similar in scale to the first generation, which is an approximate model for folding of incompetent rocks, the resulting outcrop patterns of the superposed folds, called interference patterns, have characteristic styles that depend on two angles ψ and θ. ψ is the angle between a_2, the second-generation slip direction, and S_1, the first-generation axial surface ($\psi = a_2 \wedge S_1$). θ is the angle between f_1, the first-generation fold axis, and the second-generation axial surface ($\theta = f_1 \wedge S_2$) (see Figure 12.31).

The interference patterns are shown in the right-hand diagrams in Figure 12.31*A, B,* and *C*. The first diagram in each part shows the geometry of first generation (f_1) folding. The second diagram shows the

[4] For an everyday analogue, imagine how difficult it would be to fold a sheet of corrugated sheet metal or plastic in a direction not parallel to the corrugations. The corrugations are put into the material precisely to give it flexural rigidity.

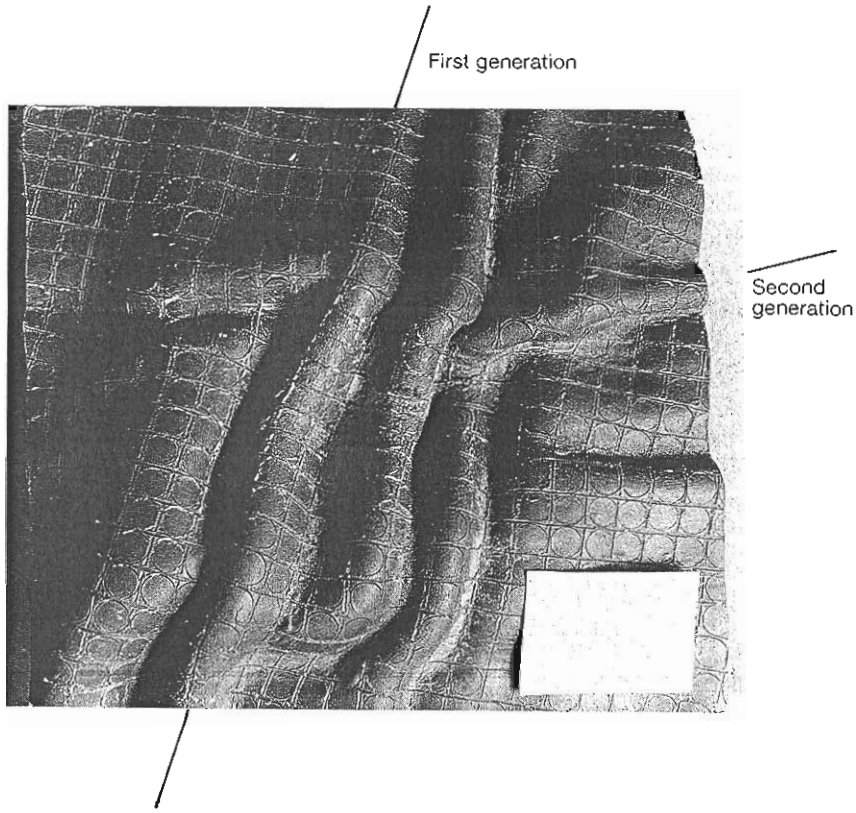

A.

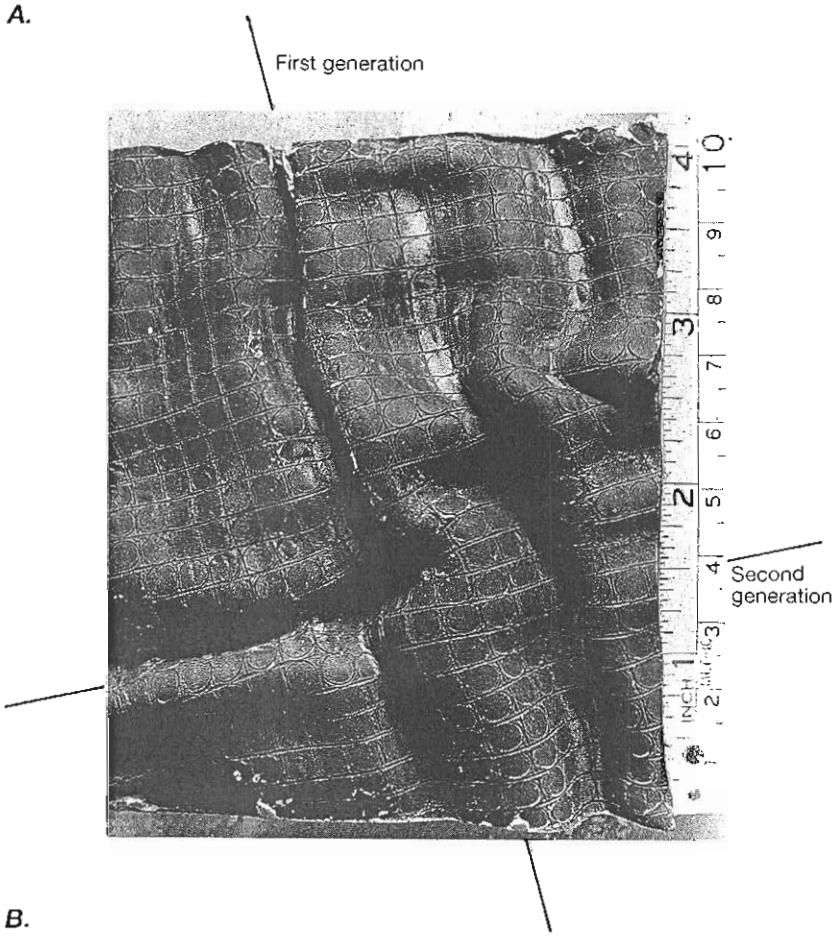

B.

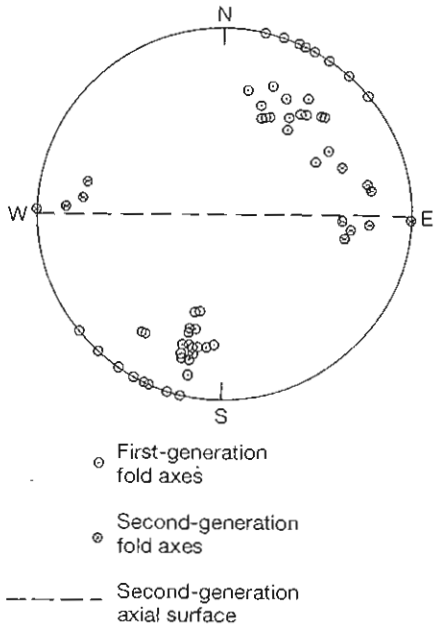

C.

Figure 12.30 Experimental models of two generations of superposed flexure folds of comparable scale. Superposed flexure folds formed by buckling a layer of competent plasticine imbedded in incompetent putty. *A*. The layers were shortened sequentially 17.5 percent and 20 percent, respectively, in two directions 70° apart. The folds trending left to right are the second generation. *B*. Sequential shortening of 17 percent and 23 percent was imposed in directions 80° apart. *C*. Stereonet projection showing first- and second-generation fold axes and poles to axial surfaces, measured from the experiment shown in part *B*.

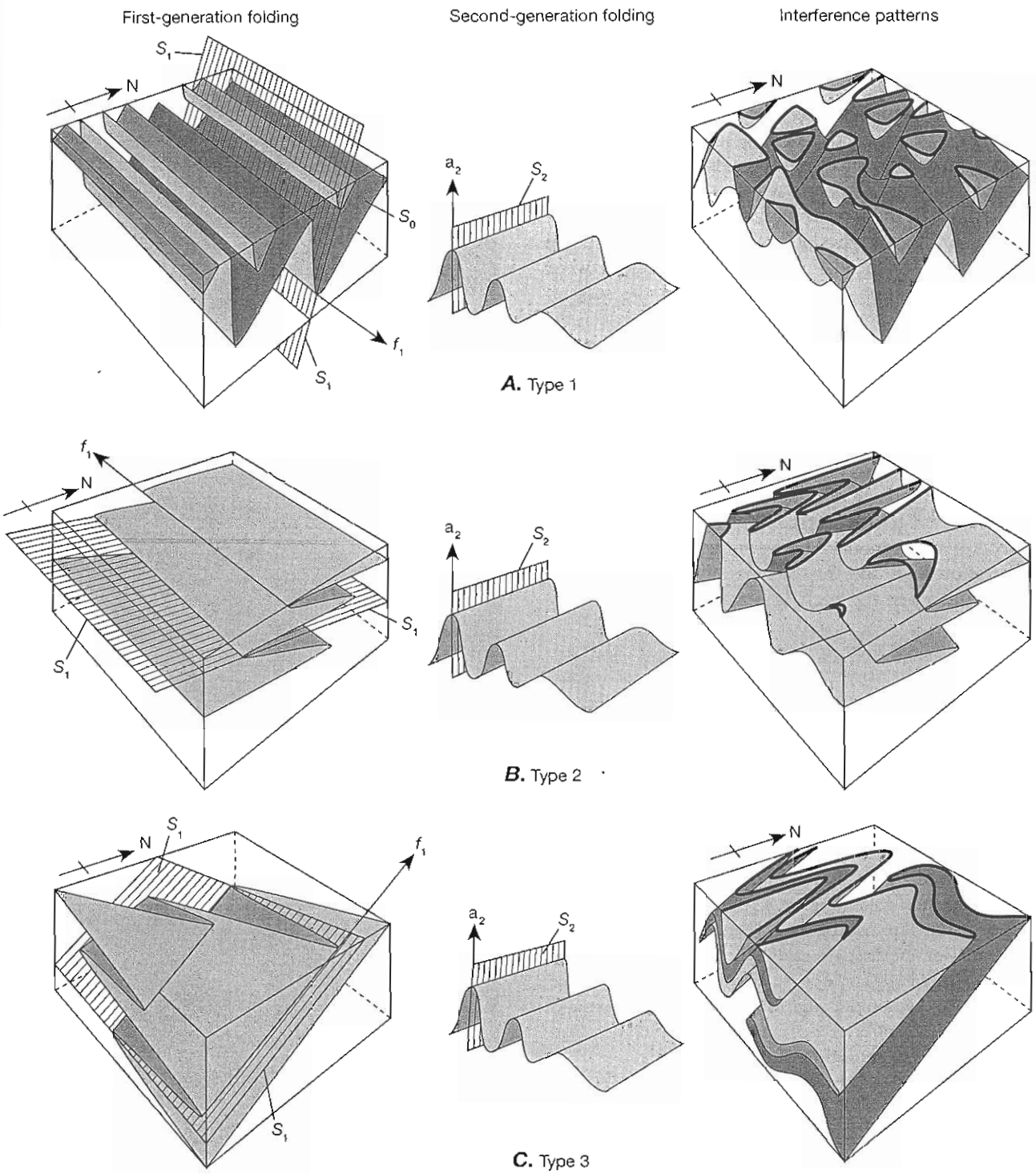

Figure 12.31 Fold interference patterns. In each case, the left-hand diagram shows first-generation folds in S_0 and the axial surface S_1; the middle diagram shows the geometry of second-generation folding as it would appear in an initially horizontal surface; the right-hand diagram shows the superposition of the second-generation folding on the folds in the left-hand diagram, with the surface eroded down to a flat plane to reveal the characteristic outcrop patterns, which are shown in heavy lines. *A*. Type 1 interference folds, showing dome-and-basin interference patterns. Here a_2 is at a small angle to S_1, and f_1 is at a high angle to S_2. *B*. Type 2 interference folds, showing arrowhead- or mushroom-shaped patterns. Here a_2 is at a high angle to S_1, and f_1 is at a high angle to S_2. *C*. Type 3 interference folds, showing the wavy outcrop pattern of the S_1 axial surface. Here a_2 is at a high angle to S_1, and f_1 is at a small angle to S_2.

geometry of the second-generation folding as it would appear in an initially horizontal surface. It is the same cylindrical fold train for *A*, *B*, and *C*. When this folding geometry is superposed on the first-generation folds, the result is the refolded folds that appear as interference patterns. The intersection of these superposed fold styles with a horizontal surface of erosion produces characteristic interference patterns, which are emphasized with heavy lines in the interference pattern diagrams.

The diffetent types of interference patterns shown in Figure 12.31 depend on two angles: the angle between the first-generation axial surface S_1 and the second-generation slip direction a_2, and the angle between the first-generation fold axis f_1 and the second-generation axial surfaçe S_2. These angles may vary from near 0° (small) to near 90° (large).

The type 1 interference folds (Figure 12.31*A*) are characterized by complete closures of the outcrop pattern of individual S_0 layers (Figure 12.32*A*). This pattern reflects the presence of domes, basins, and inrervening saddles in the folded surface. It develops when the slip direction a_2 is contained between the limbs of the first-generation folds and thus is generally at a small angle to S_1, and when the angle between f_1 and S_2 typically is large.

The type 2 interference folds (Figure 12.31*B*) are characterized by arrowhead-, crescent-, and mushroom-shaped outcrop patterns of the folded surfaces (Figute 12.32*B*). These patterns develop when the a_2 direction is not contained between the limbs of the first-generation folds and is therefore generally at a high angle to S_1, and when the angle between f_1 and S_2 typically is large, as for the type 1 pattern.

The type 3 interference folds (Figure 12.31*C*) are characterized by an undulating axial surface trace of first-generation folds (Figure 12.32*C*). This pattern develops if the slip direction a_2 is not contained between the limbs of the first-generation folds and is therefore typically at a high angle to S_1, as for type 2 interference patterns, and when the angle between f_1 and S_2 is small. These types of interference patterns are end members of a continuous gradation of patterns.

Interpretations

It is important to remember that to describe a second geueration of folds as being superposed on a first generation implies only a sequence of deformational events. It says nothing about the interval of time between those events, and it does not necessarily imply that all folds of a particular generation developed at the same time everywhere. Moteover, the same number of fold generations do not necessarily appear everywhere, so any possible correlation is probably more reliable if it is

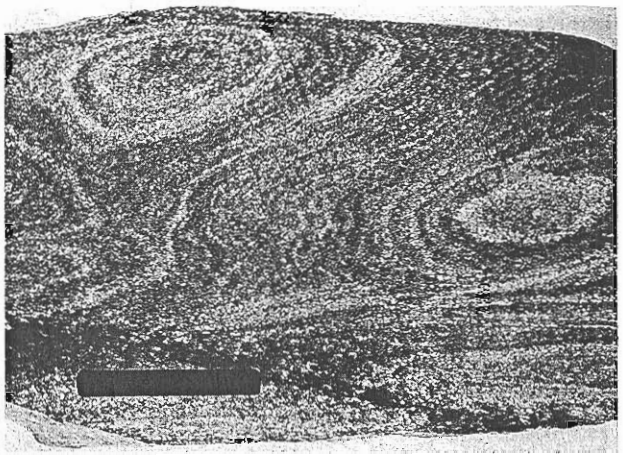

A.

B.

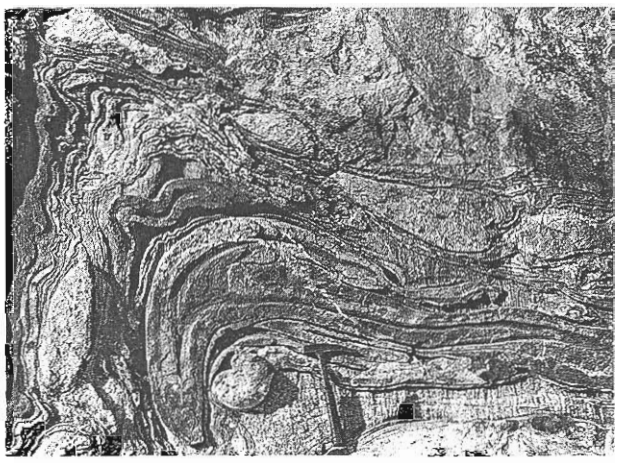

C.

Figure 12.32 Natural examples of interference fold patterns *A*. Type 1 style, showing domes and basins in a gneiss. *B*. Type 2 style developed in banded marble. C. Type 3 style developed in inrerlayered silicates and marble.

determined by fold style rather than generation number. These are very important restrictions on the interpretation of superposed folding. The deformations associated with two generations could be associated with two distinct orogenic events separated by tens or hundreds of millions of years, or they could be the result of two separate phases of a single orogenic event. In the latter case, different generations could represent separate chronological phases of a single orogeny, or they could represent changes in the geometry of deformation from place to place along the flow line for the rocks.

12.10 Diapiric Flow

Diapirs are generally circular to elliptical structures on a horizontal section that form when relatively low density rock at depth rises through overlying rock of higher density, driven by buoyant forces (the word "diapir" comes from the Greek *diapero* meaning "I pierce, I penetrate"). As the low-density material rises, there is a complementary sinking of the overlying higher-density material. The net effect is a lowering of the potential energy of the system, which makes it more stable. This process is an extremely important one in geology. It is associated with the formation of salt domes, metamorphic gneiss domes, and igneous plutons and with solid-state convective upflow in the mantle.

Salt diapirs were the first such structures to be recognized and are the best understood, in part because of their economic importance as oil traps and sources for salt and sulfur. They are widespread in areas such as the north German Plain, western Iran, the Gulf Coast region of the United States and Mexico (Figure 5.14), the southwestern Soviet Union, west central Africa, and the Canadian Arctic. Salt is deposited in oceanic basins in which circulation is very restricted, and evaporation concentrates salts in solution until they precipitate. In a rifted margin tectonic setting, salt deposits accumulate after ocean water first enters the rift but before the rift widens into an open ocean. Thus salt commonly lies at the base of a section of denser marine sediments. It can also be deposited in a restricted closing ocean basin, such as developed in late Miocene time in the Mediterranean.

Diapirs begin as anticlinal or domal uplifts and evolve into walls, columns, bulbs, or mushroom shapes (Figure 12.33). The diapirs may become detached from the original low-density layer. As the salt moves upward it pierces through the overlying sediments, which become bent upward along the margins of the diapir. These upturned sediments, truncated against the impermeable salt, provide the excellent traps for hydrocarbons that make salt domes so economically important. The tops of salt domes usually have been dissolved away by ground water (see the top of Figure 12.34C) and are characterized by broad, subhorizontal, insoluble residues from the salt and by brecciated fragments of overlying rock called the caprock. A basin commonly forms above the diapir because of the solution. The sinking of the surrounding sediments to compensate for the rise of the salt often produces a rim syncline surrounding the diapir.

When we study the structures in rocks, our only clue to the geometry of the original deformation is usu-

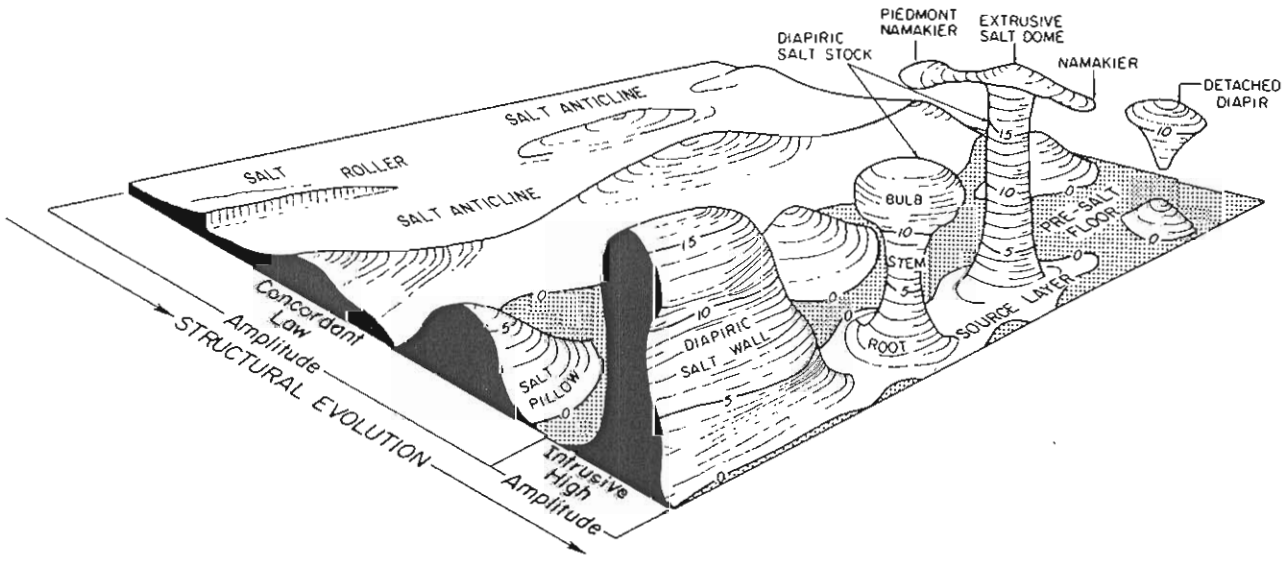

Figure 12.33 Common forms of salt intrusions. Diapirs originate from a layer of salt and then rise as salt pillows, salt stocks, or a salt wall, depending upon the extent of intrusion.

ally the geometry of features such as folds. In salt diapirs, however, we have an unusual opportunity to examine the folding that results from a fairly well undersrood pattern of flow. Such examples provide us with models rhat we can use to understand other deformational environments in which a comparable style of folding is produced.

Field relationships and models (see Section 20.7; Figures 20.19–20.21) suggest that horizontal radial flow converging toward the rising salt column initially forms a set of circumferential folds whose hinges become radially oriented (Figure 12.34*A*). Minor shifts in the flow geometry produce refolding of earlier generations of folds (lower inset, Figure 12.34*A*). As the salt moves up into the stock, the folds rorate into a vertical plunge, parallel to the main axis of rhe salt dome. A map of layers in the Grand Saline salt dome shows a complex geometry of class 2 tefolded folds and sheath folds that have subvertical to vertical hinges (Figure 12.34*B*; compare upper inset in Figure 12.34*A*). In the bulbs and mushroom caps of the domes, lateral spreading of the salt and drag along the margins causes complex refolding of the salt layers and the possible entrainment of adjacent sediments into the folds (Figure 12.34*C*).

This example shows how different generations of folds can form from a change in the flow regime along the flow path. It also illustrates that different generations of folds can form in various places at the same time. In mountain belts, therefore, one must be cautious about the significance ascribed to generations of folds.

Shale diapirs are present in some areas where folding of unconsolidated sediments has taken place or where rapid sedimentation and compaction have generated high fluid pressures in unlithified shales and caused them to move upward through the overlying rocks. The general form of these structures resembles

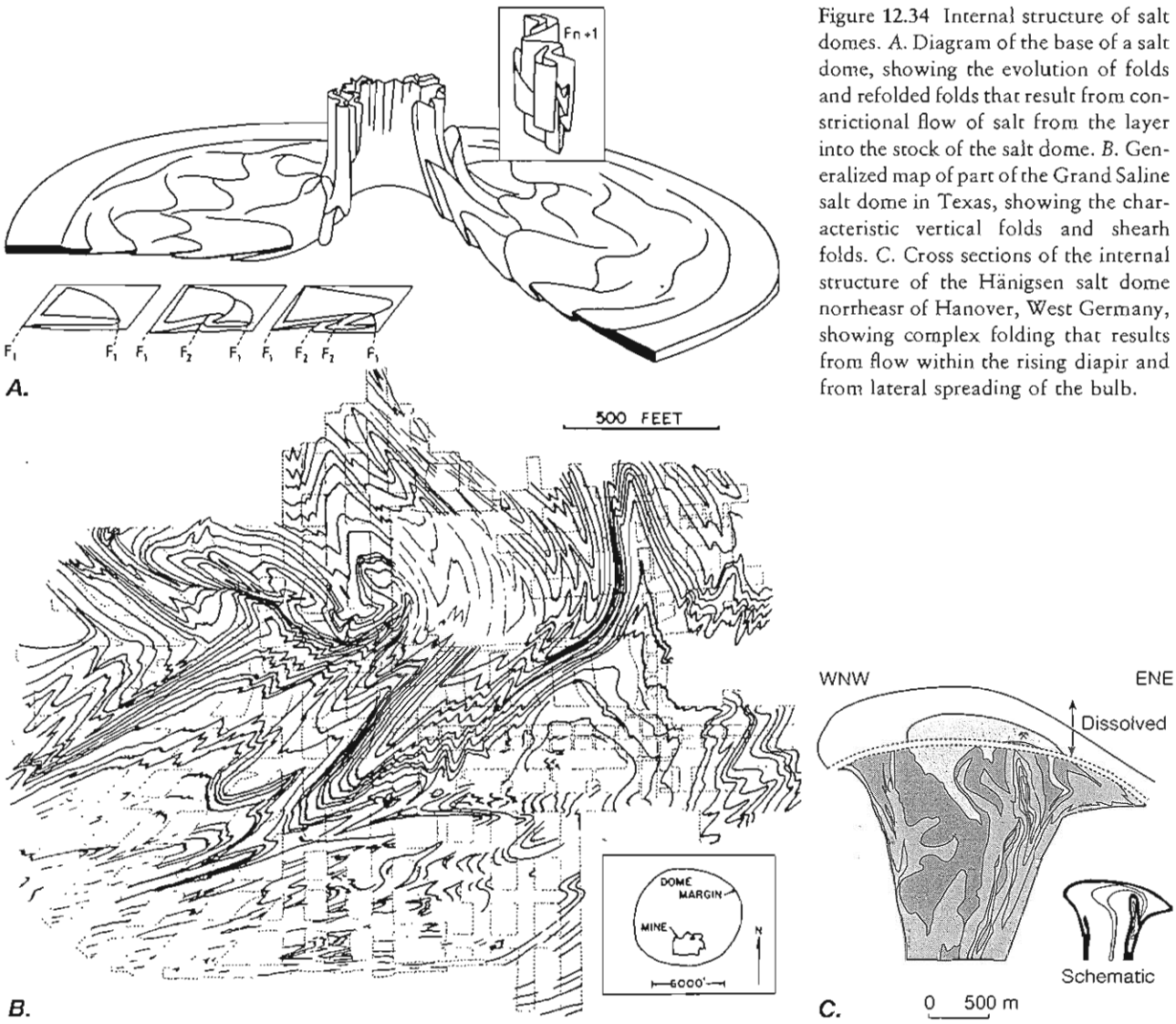

Figure 12.34 Internal structure of salt domes. *A*. Diagram of the base of a salt dome, showing the evolution of folds and refolded folds that result from constrictional flow of salt from the layer into the stock of the salt dome. *B*. Generalized map of part of the Grand Saline salt dome in Texas, showing the characteristic vertical folds and shearh folds. *C*. Cross sections of the internal structure of the Hänigsen salt dome norrheasr of Hanover, West Germany, showing complex folding that results from flow within the rising diapir and from lateral spreading of the bulb.

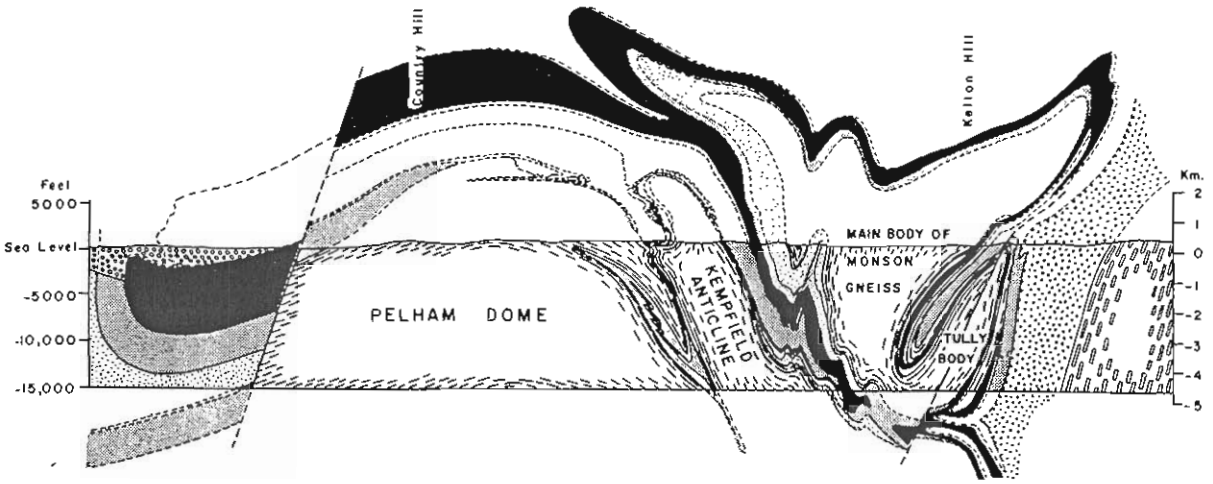

Fignre 12.35 Cross section of a gneiss dome with the mantle of deformed metasediments from the Bronson Hill Anticlinorium of west-central New England. The metasedimentary rocks were strongly deformed into recumbant nappes before deformation associated with the emplacement of the gneiss domes.

that of salt domes. In some cases the shale diapirs even reach the surface, where they form "mud volcanoes."

Mantled gneiss domes are domical bodies of gneissic rock found in highly metamorphosed core zones of orogenic belts (Figure 12.35). They commonly display foliation parallel to the walls of the body, and they are surrounded, or "mantled," by a sheath of metamorphosed sedimentary rocks. These bodies may be diapirs of gneiss intruded into overlying rocks during intense regional metamorphism.

Additional Readings

Donath, F. A., and R. B. Parker. 1964. Folds and folding. *Geol. Soc. Am. Bull.* 75: 45–62.

Grosbong, R. H. 1975. Straiu, fractures and pressure solution in natural single-layer folds. *Geol. Soc. Am. Bull.* 86: 1363–1376.

Hansen, E. 1971. *Strain facies.* New York. Springer-Verlag.

Jackson, M. P. A., and C. J. Talbot. 1989. Anatomy of musbroom-shaped diapirs. *J. Struct. Geol.* 11: 211–230.

Parterson, M. S., and L. Weiss. 1966. Experimental deformation and folding in phyllite. *Geol. Soc. Am. Bull.* 77: 343–374.

Ramsay, J. G. 1967. *Folding and fracturing of rocks.* New York: McGraw-Hill.

Skjernaa, L. 1975. Experiments on superimposed buckle folding. *Tectonophysics* 27: 235–270.

Suppe, J. 1983. Geometry and kinematics of fault bend folding. *Am. Jour. Sci.* 283: 684–721.

Snppe, J. 1985. *Principles of structural geology.* Englewood Cliffs, N. J.: Prentice-Hall.

Talbot, C. J., and M. P. A. Jackson. 1987. Internal kinematics of salt diapirs. *Am. Assoc. Petrol. Geol. Bull.* 71 (9): 1068–1093.

Thiessen, R. L., and W. D. Means. 1980. Classification of fold interference patterns: A reexamination. *J. Struct. Geol.* 2: 311–316.

Weiss, L. E. 1980. Nuclearion and growtb of kink bands. *Tectonophysics* 65: 1–38.